Nonhydrostatic simulations of the regional circulation in the Monterey Bay area

Yu-Heng Tseng[1] and L. C. Breaker[2]

Received 15 January 2007; revised 21 June 2007; accepted 31 August 2007; published 25 December 2007.

[1] The regional circulation in the vicinity of Monterey Bay is complex and highly variable. We use a one-way coupled, nonhydrostatic version of the Dietrich Center for Air Sea Technology (DieCAST) ocean model to simulate the regional circulation. Seasonally varying local wind stress, topographic irregularities, coastal upwelling, and forcing from the open ocean are all important in this region. Satellite imagery often shows a cyclonic eddy inside the bay and an anticyclonic eddy outside the bay. The offshore anticyclonic eddy is also associated with a year-round anticyclonic eddy over the Monterey Submarine Canyon (MSC). The offshore eddy is better organized during winter. It is found that the California Undercurrent (200–400 m) does not enter the bay itself but is diverted offshore past the entrance of the bay, presumably to reform farther north along the coast. The main branch flows northward contributing to the deep anticyclonic eddy located approximately 50 km offshore of Monterey Bay. The simulations show that vertical motion is greater during summer than winter, as expected. During spring upwelling, the deep waters often upwell along the walls of the canyon and then spread and mix with surrounding waters. The deep circulation enhances mixing significantly due to the topography. We further investigate the regional circulation by comparing it with the cases where the deep canyon was filled gradually. Vortex stretching over the canyon just beyond the entrance to Monterey Bay and along the adjacent continental slopes contributes to cyclonic circulation at deeper levels. Vertical sections of velocity along the axis of MSC indicate horizontal and vertical patterns of flow that are generally consistent with past observations on the circulation of Monterey Bay.

Citation: Tseng, Y.-H., and L. C. Breaker (2007), Nonhydrostatic simulations of the regional circulation in the Monterey Bay area, *J. Geophys. Res.*, *112*, C12017, doi:10.1029/2007JC004093.

1. Introduction

[2] Monterey Bay is located 100 km south of San Francisco between 36.5° and 37°N along the central California coast. Many observational studies have examined its circulation and related processes due in part to its high biological productivity [e.g., *Rosenfeld et al.*, 1994; *Breaker and Broenkow*, 1994; *Ramp et al.*, 1997; *Collins et al.*, 2000; *Breaker*, 2005]. This region is highly variable and consists of several different water masses. Theoretical and modeling studies off the coast of California have often focused on coastal upwelling and related processes in response to the prevailing equatorward winds over the continental shelf. More recently, many filaments associated with the equatorward flowing California Current (CC) are found to stream offshore from coastal promontories, based on satellite and drifters observations [e.g., *Collins et al.*, 2000]. Observations indicate that the variability of the circulation in this region plays an important role in cross-shore transport with implications for fisheries, water quality, shoreline morphology, and shipping.

[3] Coastal upwelling is observed frequently in the Monterey Bay area, although not within the bay itself. The bay breaks the continuity of the equatorward flow that develops in response to coastal upwelling. In areas where upwelling favorable winds occur, vertical motion is greatly enhanced. When cold and dense water is upwelled to the surface, an upwelling front typically forms and a density inversion subsequently develops. It is found that hydrostatic models can not satisfactorily reproduce the density inversion and resulting instability because these effects are essentially nonhydrostatic [*Hodges et al.*, 2006; *Fringer and Street*, 2003]. In a hydrostatic model the parameterization for vertical mixing stabilizes the water column instantaneously and creates a local mixed zone (T. Du et al., Impacts of tidal currents and Kuroshio Intrusion on the generation of nonlinear internal waves in Luzon Strait, manuscript in preparation for *Journal of Geophysical Research*, 2007), and thus the unresolved surface mixed layer may be problematic. In previous work we found that mixed baroclinic and barotropic instabilities and modified Rayleigh-Taylor instabil-

[1]Department of Atmospheric Sciences, National Taiwan University, Taipei, Taiwan.
[2]Moss Landing Marine Laboratory, Moss Landing, California, USA.

0148-0227/07/2007JC004093

ities contribute significantly to the development of filaments and meanders resulting from the upwelled waters off the U.S. west coast [*Tseng and Ferziger*, 2001]. Thus the development of filaments and frontal eddies in regions of coastal upwelling are better represented by a nonhydrostatic model due to a more accurate representation of the vertical velocity field. *Chao and Shaw* [2002] further verified that nonhydrostatic models enhance the growth of the coastal upwelling meanders and filaments in upwelling simulations. Recently, *Tseng et al.* [2005] also found that nonhydrostatic contributions to the vertical field of motion off Point Sur and near the Monterey Submarine Canyon (MSC) became important where bottom slopes changed rapidly. These results motivate us to further investigate the dynamics of this area and the influence of MSC on the local circulation using a nonhydrostatic model.

[4] Topographic effects on the wind-driven coastal circulation have been studied by *Narimousa and Maxworthy* [1989]. Their results indicate that where local upwelling centers occur, standing waves and offshore Ekman transport are produced. Submarine canyons are also known to be important in determining the nature of the coastal circulation [e.g., *Klinck*, 1996; *Hickey*, 1997; *She and Klinck*, 2000]. *Hickey* [1997] studied the spatial patterns of the three-dimensional velocity and temperature fields of Astoria Canyon and deduced vorticity patterns resulting from upwelling/downwelling-favorable winds. The observations of *Hickey* [1997], however, lack important three-dimensional features and the related dynamics. *She and Klinck* [2000] applied a hydrostatic primitive equation model to a smoothed version of Astoria Canyon. Their results are consistent with the results of *Hickey* [1997] for steady upwelling/downwelling-favorable winds. However, quantitative replication of Hickey's results was difficult to obtain due to its idealized model setting.

[5] *Allen et al.* [2003] also studied upwelling in a laboratory setting over simplified submarine canyons using the S-Coordinate Rutgers University Model [*Song and Haidvogel*, 1994]. Poor agreement was found between the laboratory experiments and numerical models due to nonhydrostatic effects, for homogeneous cases, and vertical advection errors, for stratified cases. The advection errors are not due to the pressure terms investigated previously [*Haney*, 1991] but rather are due to errors in vertical advection of the density field. The numerical errors result from the terrain-following coordinates combined with a strong vertical gradient in density, vertical shear in the horizontal velocity, and complicated topography [*Allen et al.*, 2003]. Their comparisons show that hydrostatic, σ-coordinate models are not adequate when baroclinic modes dominate the flow in areas with steep slopes.

[6] The regional circulation in the Monterey Bay area is highly correlated with coastal upwelling along the open coast just north of the bay. It is also influenced by the local topography, and is tightly coupled to the California Current System (CCS). Many of the early numerical studies used simplified geometry, bottom topography, and surface/boundary forcing [e.g., *Bruner*, 1988; *Ly and Luong*, 1999; *Petruncio et al.*, 2002]. These studies often failed to accurately simulate the complex circulation in this region using realistic topography and stratification until data assimilation was included [*Shulman et al.*, 2002; *Paduan and Shulman*, 2004].

[7] Recently, a triply nested version of the Regional Ocean Modeling System (ROMS) for the California coast was used to produce three-dimensional (3-D) ensemble forecasts of the Monterey Bay area during August 2003 as part of the Autonomous Ocean Sampling Network-II (http://www.mbari.org/aosn). It represents an integration of multiple observing platforms, data assimilation schemes and high-resolution numerical models of the coastal ocean. *Li et al.* [2006] further developed the ROMS in this area to emphasize the capability for predicting mesoscale to small-scale variability. These models were successful in predicting the short-term regional circulation. However, the complicated MSC bathymetry in these models was filtered, resulting in possible underpredictions of the intensity of the local currents and the full influence of the canyon.

[8] Many numerical studies have considered flow near coastal irregularities off the west coast of the United States. However, no study has explicitly focused on the interaction of a strong upwelling jet with a coastal feature such as Monterey Bay. *Tseng et al.* [2005] coupled a regional model to a larger-scale CCS model, which was shown to have an impact on the regional circulation in the Monterey Bay area. Similarly, *Penven et al.* [2006] used a one-way coupled model to show that a realistic regional ocean model could completely resolve eddies in the presence of steep bathymetry without topographical smoothing for shallow coastal processes that have short length scales.

[9] The goals of the current work are to apply a high-resolution, nonhydrostatic coastal ocean model to simulate the coastal dynamics in the Monterey Bay area without data assimilation and to investigate the effects of realistic, steep bathymetry on the coastal circulation. Nonhydrostatic simulations have emerged popularly to study this area because of the complexity of MSC on the local circulation and internal wave generation [e.g., *Tseng et al.*, 2005; *Jachec et al.*, 2006]. The importance of internal waves will not be addressed in this study due to the different range of timescales. This paper is organized as follows. Section 2 introduces the high-resolution Monterey Bay area regional model. Section 3 presents the simulation results. Section 4 illustrates the effects of MSC on the larger-scale circulation. Finally, conclusions are drawn in section 5.

2. Monterey Bay Area Regional Model (MBARM)

[10] In order to study the regional circulation in the vicinity of Monterey Bay, we use the nonhydrostatic version of the MBARM. The model is based on the z-level, fourth-order accurate Dietrich Center for Air Sea Technology (DieCAST) ocean model, which provides high computational accuracy and low numerical dissipation and dispersion [*Dietrich*, 1997]. The MBARM is one-way coupled to a larger-scale CCS model [*Haney et al.*, 2001] and uses the immersed boundary method to represent the coastal geometry and bathymetry [*Tseng and Ferziger*, 2003, 2004; *Tseng et al.*, 2005].

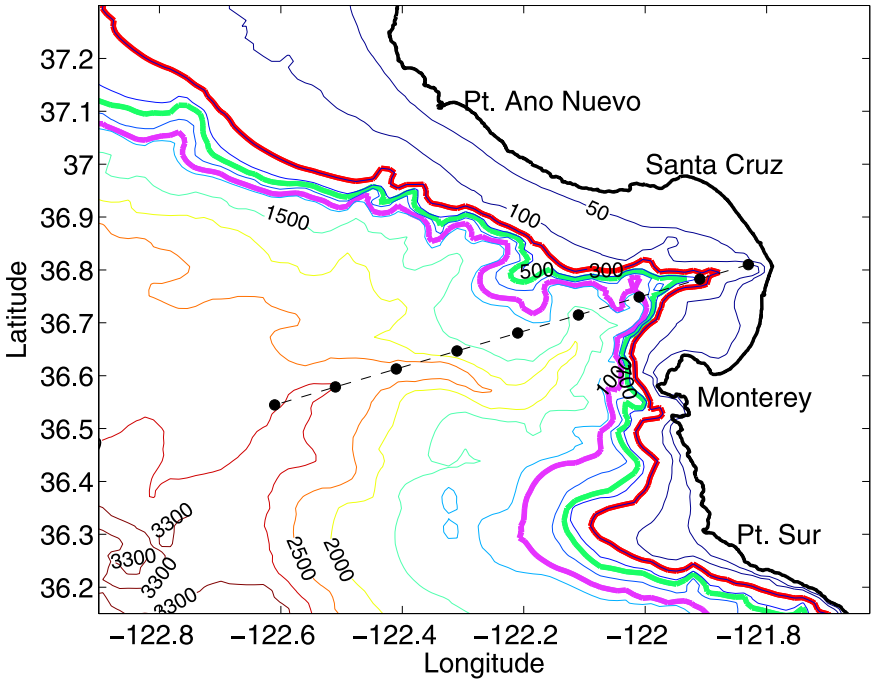

Figure 1. Model domain of MBARM and bathymetry. Dashed line cuts through the Monterey Canyon. Every 20 km is shown by a black circle. The solid red, green, and pink lines represent the bathymetry at 300, 580, and 880 m depth.

2.1. Model Description

[11] The model uses a blend of collocated and staggered grid structures (mixed Arakawa A and C grids). The Coriolis terms are evaluated on the "A" grid and thus have no spatial interpolation error [*Dietrich*, 1997]. The governing equations and numerical procedures are given in detail by *Tseng et al.* [2005] and will not be repeated here. A detailed model description and the nonhydrostatic solver can also be found in the work of *Tseng* [2003] and *Dietrich and Lin* [2002]. Fourth-order central differencing is used in the control volume approximation to compute all advection and horizontal pressure gradient terms, except adjacent to boundaries where second-order accuracy is used. Accurate, low-dissipation numerics are required in order to simulate the coastal eddies that dominate the circulation in Monterey Bay. This low-dissipation requirement is clearly justified in the results of *Tseng and Dietrich* [2006]. In addition, with the application of a nonhydrostatic model, it is possible that improved estimates of vertical velocity will be obtained since all of the terms in the vertical equation of motion are retained.

[12] The model uses a rigid-lid approximation, which is appropriate for "slow modes" in the general circulation [*Smith et al.*, 1992; *Dukowicz et al.*, 1993]. Use of a rigid lid excludes the "fast modes" associated with barotropic free surface waves. The rigid-lid approximation does not affect internal gravity wave speeds. Thus it does not affect geostrophic adjustment of the baroclinic modes that dominate the regional circulation. The rigid-lid approximation also simplifies the treatment of open boundaries by greatly reducing the range of frequencies that must be addressed.

[13] Density is determined from a nonlinear equation of state relating density to potential temperature, salinity, and a reference pressure. The MBARM results are based on the bathymetry from *Wong and Eittreim* [2001]. The filters used in some models which smooth the bathymetry may result in underpredicting the intensity of the coastal currents and eddies. This in turn results in weaker coastal eddies as the CCS interacts with the filtered bathymetry and smoothed coastlines. We believe that the use of realistic bathymetry in the MSC is unique and sets apart the results of this study from previous modeling work in Monterey Bay.

2.2. Model Implementation

[14] The domain of MBARM extends from 36.1° to 37.4°N and from the California coast out to 122.9°W (Figure 1); the horizontal grid size is 1/72° (∼1.5 km) in longitude and latitude. A grid sensitivity study shows similar circulation patterns for an even higher resolution grid (1/108°), implying that the current resolution is sufficient to resolve the offshore eddies and details of the local circulation [*Tseng et al.*, 2005]. The vertical grid has 28 levels and is exponentially stretched to resolve surface boundary layers with a 10 m thickness in the top layer.

[15] The surface buoyancy flux is computed by nudging both temperature and salinity toward *Levitus*' [1982] monthly climatology. This is equivalent to adding heat and/or freshwater to the top layer. The wind stress is from *Hellerman and Rosenstein*'s [1983] 1° × 1° monthly climatology. Spline interpolation is used in the model to ensure the change of surface forcing is gradual. This surface forcing is chosen for consistency with the coupled larger-scale CCS model [*Haney et al.*, 2001]. The current resolution of wind forcing can adequately resolve the important features of the circulation in this area. However, a higher-resolution nearshore wind field is required to produce more realistic flow structure and predictions adjacent to the coast

[*Pickett and Paduan*, 2003]. We will further explore the issue of wind forcing sensitivity in a following study. Vertical viscosity and diffusivity are the sum of the terms which parameterize laminar diffusivity and the vertical Reynolds stresses as given by *Pacanowski and Philander* [1981]. The horizontal eddy viscosity and diffusivity are 20 m^2/s. This gives a damping time of nearly a month for disturbances on the scale of 10 km. The bathymetry is the unfiltered USGS 250 m resolution topography of *Wong and Eittreim* [2001]. The sea floor is insulated and a no-slip boundary condition is applied with a bottom drag coefficient of 0.002. The MBARM is run for 10 years to make sure it reaches its quasi-steady state for at least several years [*Tseng et al.*, 2005]. We present the results from the eighth year of 10-year simulation.

2.3. Lateral Open Boundaries

[16] In order to focus on the regional circulation without requiring extensive computational resources, we couple the local domain to a larger-scale model through lateral open boundaries. The MBARM is one-way coupled to the larger-scale CCS model of *Haney et al.* [2001] which has a resolution of 1/12°. To simplify the analysis and minimize artificial effects at the open boundaries, the year 3 results from the CCS model are used to force the open boundaries, and all quantities are interpolated from the daily CCS model output and updated every time step (40 s). The CCS model uses the same climatological forcing. The MBARM is initialized using interpolated values from the coarse CCS results after 2 a of simulation. All open boundary conditions are based on boundary fluxes. A pure upwind advective scheme is used at the three lateral open boundaries (north, south, and west) for all variables. The open boundaries allow perturbations generated inside the MBARM domain to leave without deterioration of the model solution and also allow the CCS model information to advect inward. The CCS model results are advected inward as an inflow boundary condition, and the interior model results are advected outward as an outflow boundary condition. Net lateral boundary flow through the open boundary is adjusted at every time step such that there is no net inflow into the model domain which is required by incompressibility, that is, volume conservation. The MBARM model does not use sponge layers, which dissipate the errors generated by overspecification of the boundary conditions. These open boundary conditions have also been applied in two-way coupling studies in the North Pacific Ocean, North Atlantic Ocean, and Mediterranean Sea [e.g., *Dietrich et al.*, 2004; *Jan et al.*, 2006; D. E. Dietrich et al., Mediterranean overflow water (MOW) simulation using a coupled multiple-grid Mediterranean Sea/North Atlantic Ocean model, manuscript in preparation for *Journal of Geophysical Research*, 2007]. Further details of the open boundary treatment are discussed by *Tseng et al.* [2005].

3. Simulation Results

[17] As stated earlier, our goals are to examine the seasonal flow and its variability in the vicinity of Monterey Bay using climatological forcing and realistic topography and to investigate the impacts of MSC on upwelling and the local circulation. We also explore the fate of the deep water that is upwelled in the canyon to determine if it reaches the surface or spreads out onto the shelves contributing to the adjacent shelf bottom waters before eventually reaching the surface.

3.1. Seasonal Variability

[18] The model simulations reproduce many important features of the observed annual cycle of the CCS including the strengthening of the shallow equatorward jet in spring and the weakening of the jet in autumn. A description of the annual mean flow and the general circulation based on earlier model results has been given by *Tseng et al.* [2005]. We further examine the seasonal variability here. The seasonal variability is closely associated with the spring transition to coastal upwelling and the fall transition that signals the arrival of the Davidson Current [*Breaker*, 2005]. Figures 2–3 show the summer and winter mean velocity fields at depth of 10.1, 50, 100, 200, 300, and 400 m for the eighth year of the 10-year simulation. Vertical velocities are represented by the color contours (in meters/week). The summer period as May through August and the winter period is defined as November through February. The alongshore component of the wind stress has been shown to be a key factor in generating the surface equatorward and subsurface poleward undercurrents. Strong vertical and horizontal shears and opposing flows are observed at different depths in both seasons. Strong vertical (i.e., baroclinic) and horizontal (i.e., barotropic) shears are observed in the upper 100 m. These currents are often baroclinically and barotropically unstable, resulting in the generation of meanders, filaments, and eddies. In the spring the equatorward flow strengthens and becomes dominant from the surface to a depth of 100 m. This equatorward flow is forced by the climatological upwelling-favorable winds. A weak cyclonic eddy is observed inside Monterey Bay to 50 m during summer and is associated with the bifurcated equatorward flow that occurs at the entrance of MB [*Rosenfeld et al.*, 1994]. There is also a large-scale, anticyclonic eddy slightly further offshore approximately 50 km from the coast that extends down to 400 m. This feature is better developed in winter. There is subsurface northward flow below depths of 200 m consistent with the year-round poleward flow associated with the California Undercurrent (CUC). The transition from equatorward surface flow to deeper flow in the CUC occurs between depths of 100–400 m and the strongest flow in the CUC occurs at depths of 200–300 m, consistent with previous observations [e.g., *Hickey*, 1979]. Coastal upwelling is clearly observed from the large mean upward vertical velocities (orange) near the coast and is associated with downwelling (green) further offshore. It is clear that vertical motions are greater during summer than winter. They are most pronounced at depths of 50–200 m, but upward motion can be observed as deep as 300 m. The downwelling occurs further offshore in a band that parallels the upwelling and suggests vertical cell-like circulation as described by *Mooers et al.* [1976] off the coast of Oregon. This downwelling region is closely related to the upwelling front that migrates offshore in summer. Finally, our results indicate that the CUC (200–400 m) does not enter the bay itself but is diverted offshore past the entrance of the bay, presumably to reform further north along the coast.

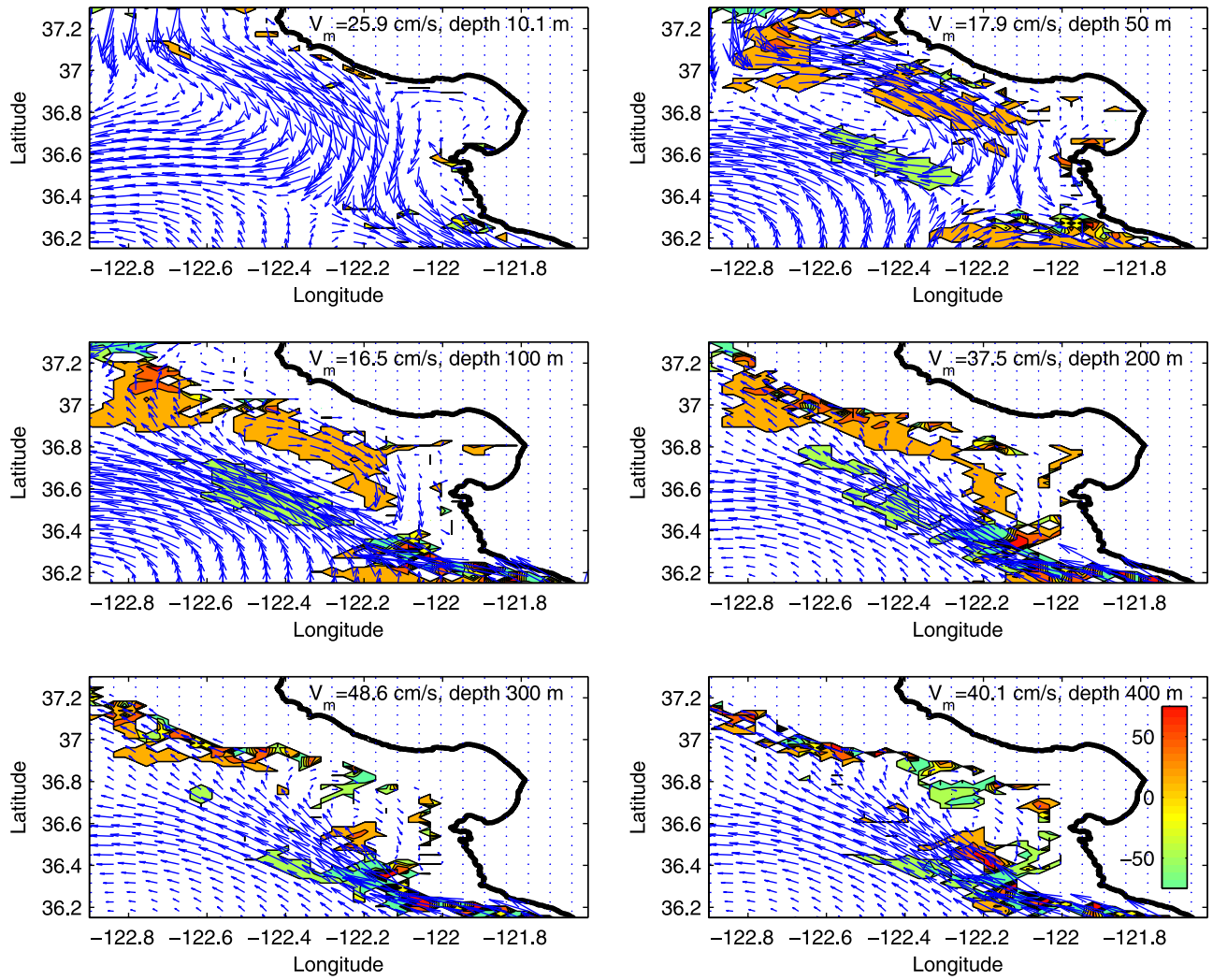

Figure 2. Mean velocity field at various depths during summer (May to August) at depth (a) 10.1 m, (b) 50 m, (c) 100 m, (d) 200 m, (e) 300 m, and (f) 400 m. The unit of vertical velocity in the color bar is meters/week.

[19] In summer, the southward flow at upper levels tends to move offshore, forming the filaments frequently observed in satellite imagery. Point Año Nuevo and Point Sur, both upwelling centers, are the locations where the offshore flow often occurs. Figure 4 shows an extended filament off Point Año Nuevo during summer and offshore waters entering the bay during winter. These features are also associated with larger vertical velocities during summer, consistent with the observations of *Ramp et al.* [1997].

[20] Between November and February, the dominant flow changes from equatorward to poleward in the upper ocean (Figure 3). By mid-October, coastal upwelling occurs much less frequently, and near-surface flow along the central coast is under the influence of the poleward flowing Davidson Current (DC), which generally reaches its maximum speed at the surface in December [*Paduan and Rosenfeld*, 1996]. Significant upward motion along the coast is not observed. However, we still find upward motion associated with the CUC over the Sur Ridge. *Tisch et al.* [1992] found poleward geostrophic flow throughout the water column in a narrow band inshore of the anticyclonic eddy in November 1988 off Point Sur, a feature which is not well depicted in our simulations. The seasonally averaged velocity fields during winter show that the northward flow is most intense near the surface but occurs at all depths. This northward flow represents the DC and the CUC, and so during this period it is not possible to distinguish between them. The model intensification of the CUC and DC agrees well with observations [e.g., *Collins et al.*, 2000]. Finally, we assume that the CUC/DC reform north of Point Año Nuevo, but our model domain is not large enough to determine their fate further north.

[21] The velocity fields in winter at all levels show different spatial structure than those in summer. The flow is strongly poleward south of MB. Equatorward flow can still be observed further north and offshore only from 10 to 100 m. Their interaction increases the horizontal shear which may enhance offshore transport. The offshore eddy field is well organized, but, there is still see evidence of weak northward flow along the coast between MB and Point Año Nuevo to depths of 50 m. The DC (down to 50 m) off Point Sur usually flows to the northwest, while the

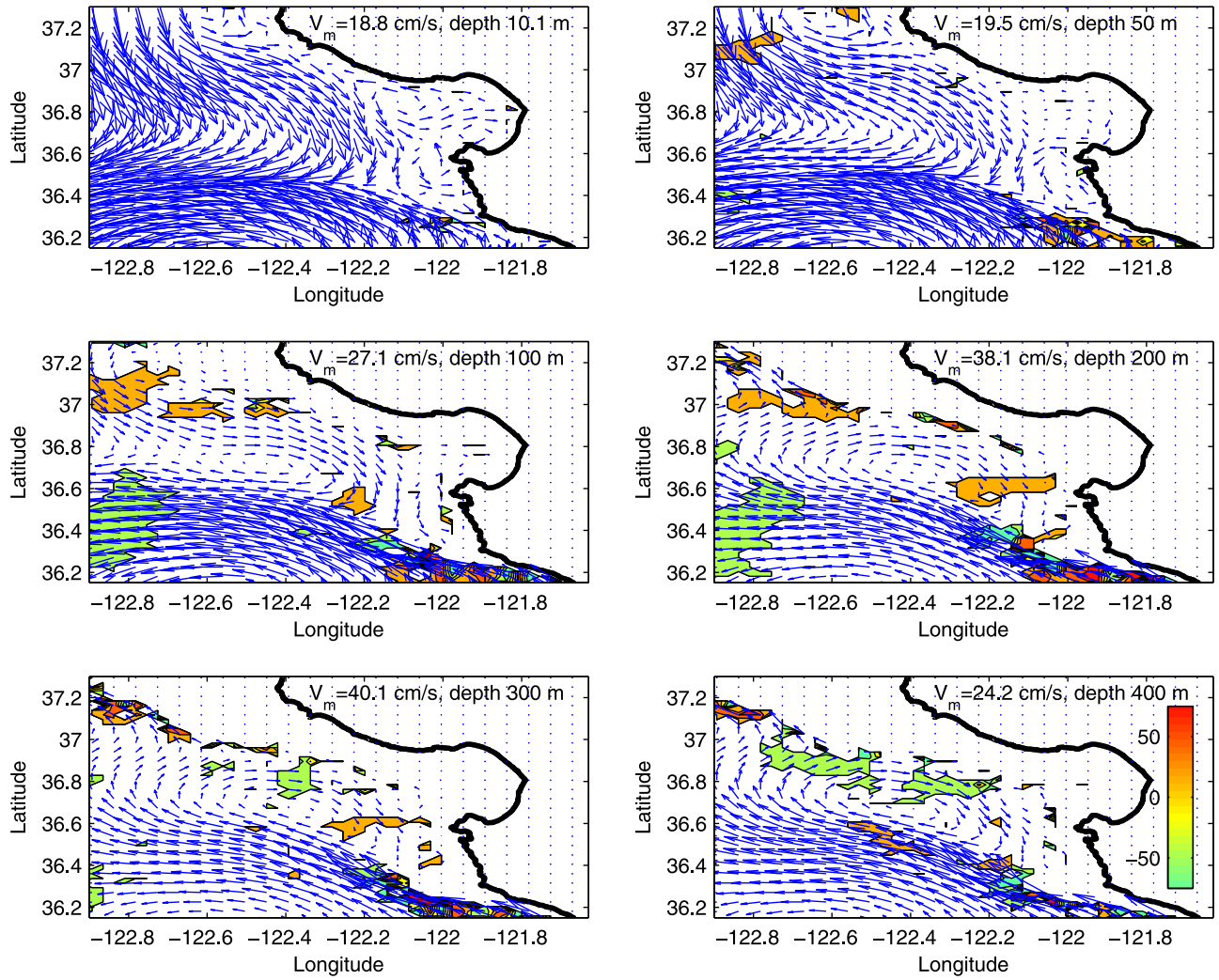

Figure 3. Mean velocity field at various depths during winter (November to February) at depth (a) 10.1 m, (b) 50 m, (c) 100 m, (d) 200 m, (e) 300 m, and (f) 400 m. The unit of vertical velocity in the color bar is meters/week.

summer equatorward flows are toward the southwest (Figure 2). These features are attributed to the steering effects of the local topography. The results also confirm the presence of a quasi-permanent anticyclonic eddy offshore of Monterey Bay at depth year-round, a feature that appears to be better organized during winter. Our results suggest that this eddy is directly associated with the interaction of the CCS and the local topography.

[22] Sea surface temperature (SST) fields for different seasons (day 110 of year 8-spring, day 200-summer, day 290-autumn, day 20 of year 9-winter, every 90 d) are shown in Figures 4a–4d. In spring, when upwelling-favorable winds intensify, filaments of cold water that originate near the coast begin to move offshore. In Figure 4a a filament of cold upwelled water extends toward the southwest corner of the domain. The patterns and boundaries depicted indicate that upwelling fronts are formed during this period. The coastal eddy fields and filaments by late summer propagate offshore as the upwelling-favorable winds diminish along the coast. In Figure 4c the cold filaments propagate further offshore and the SST field becomes warmer up by autumn (note that the color scales are different in Figure 4 to accommodate the range of temperatures during each season). The SSTs show that swirling patterns with eddy-like features and offshore filaments dominate the circulation, reminiscent of the patterns depicted in infrared and ocean color satellite imagery of this area. Winter is marked by warmer SSTs as the offshore waters tend to move shoreward toward Monterey Bay (Figure 4d).

[23] In summary, the seasonal cycle is characterized by the onset of coastal upwelling and the formation of surface baroclinic jets in the spring shortly after the upwelling-favorable winds are established. Instabilities often develop along the jet, and the entire field (jets and eddies) propagates offshore during summer and autumn. During the period of coastal upwelling, northward flow within the bay results from the bifurcated flow indicated by *Rosenfeld et al.* [1994]. Most filaments occur in spring and summer, forming cold and warm mushroom-like patterns at multiple scales, especially south and north of Monterey Bay where upwelling centers are located. In autumn and winter, meanders and eddies are frequently observed, both near the coast

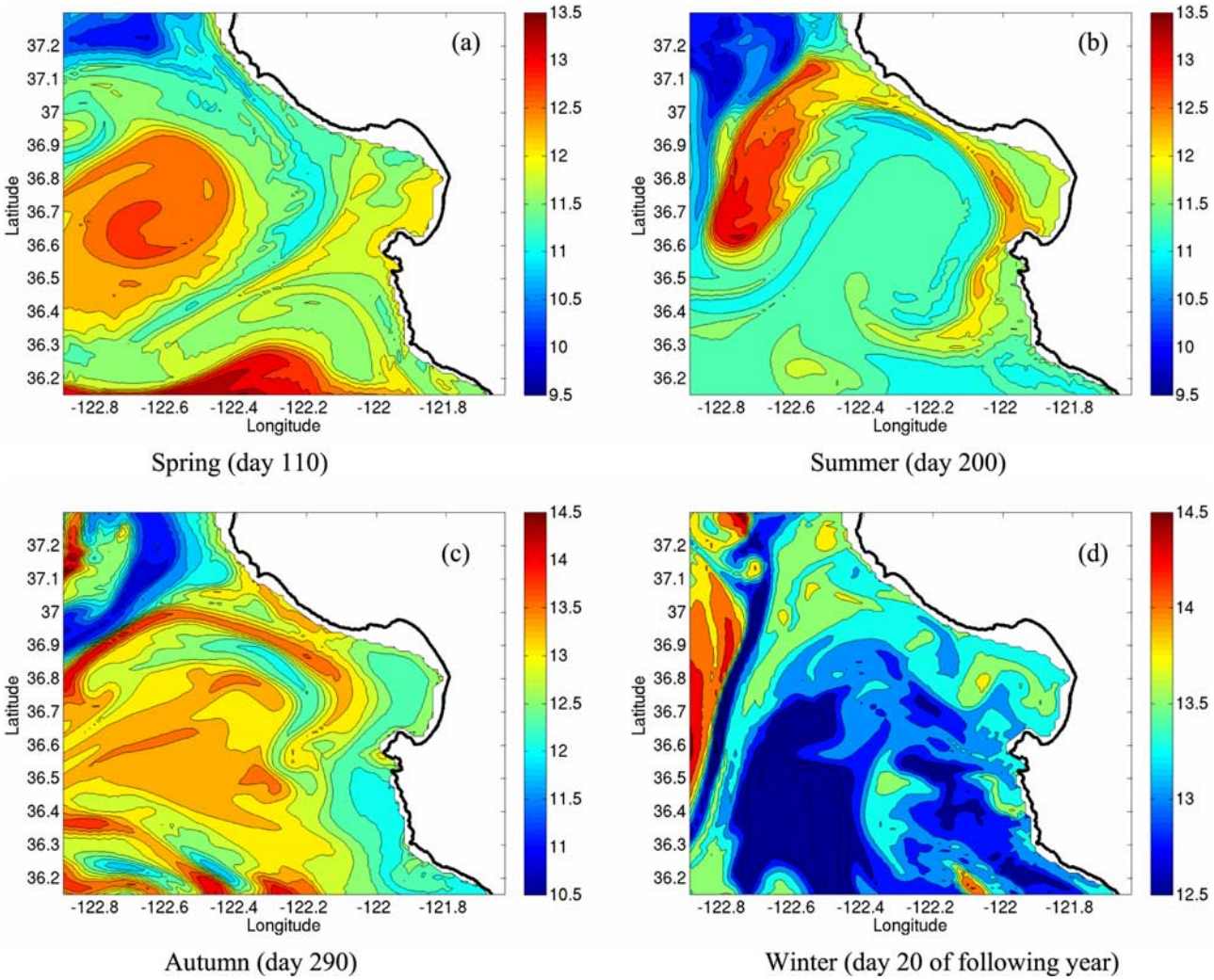

Figure 4. Sea surface temperature in different seasons, with (a) spring (day 110); (b) summer (day 200); (c) autumn (day 290); (d) winter (day 20 of following year).

and further offshore. Finally, the prevailing surface circulation in Monterey Bay, although weak compared to the flow offshore, is generally northward throughout the year consistent with previous results [e.g., *Breaker and Broenkow*, 1994].

3.2. Upwelling In and Around Monterey Bay

[24] On the basis of the climatological annual cycle of SST, spring and early summer are the coolest times of the year mainly due to the onset of coastal upwelling. The deeper temperatures (100 m) reach a minimum in June, slightly later than SST and more in phase with the Bakun upwelling index [*Tseng et al.*, 2005]. The water column is nearly unstratified to depths of ~50 m. The upwelling signal is evident in the currents and temperatures in our simulations shown in Figure 4. *Rosenfeld et al.* [1994] identified upwelling at Point Año Nuevo, north of Monterey Bay, as the source of cold, higher salinity, near-surface water that is advected south under the influence of the equatorward jet and is frequently seen in the Bay. The circulation in the vicinity of Monterey Bay during spring and summer when strong upwelling-favorable winds are present is characterized by strong near-surface horizontal temperature gradients and higher biological productivity. Upwelling is initially confined to a narrow region adjacent to the coast with a length scale approximated by the internal Rossby radius. As upwelling progresses, an Ekman layer with strong vertical shear develops and then propagates away from the coast on seasonal timescales [*Breaker and Mooers*, 1986].

[25] Figure 5 shows daily averaged vertical velocities along a vertical section cut through the center of MSC (dash line in Figure 1) during strong spring upwelling starting from day 90 of year 8. Spring upwelling is generated by the intensified equatorward surface winds during spring in the surface wind climatology [*Hellerman and Rosenstein*, 1983]. Upward vertical velocities >+0.1 cm/s are marked in red while downward velocities <−0.1 cm/s are marked in blue. The contour interval is 0.005 cm/s. Velocities of these magnitudes have been reported before [e.g., *Breaker and Broenkow*, 1994] and can raise deep water several hundred meters in a single day. Upward vertical motion is frequently seen along the canyon axis. Larger upward vertical velocities occur both inside MB and

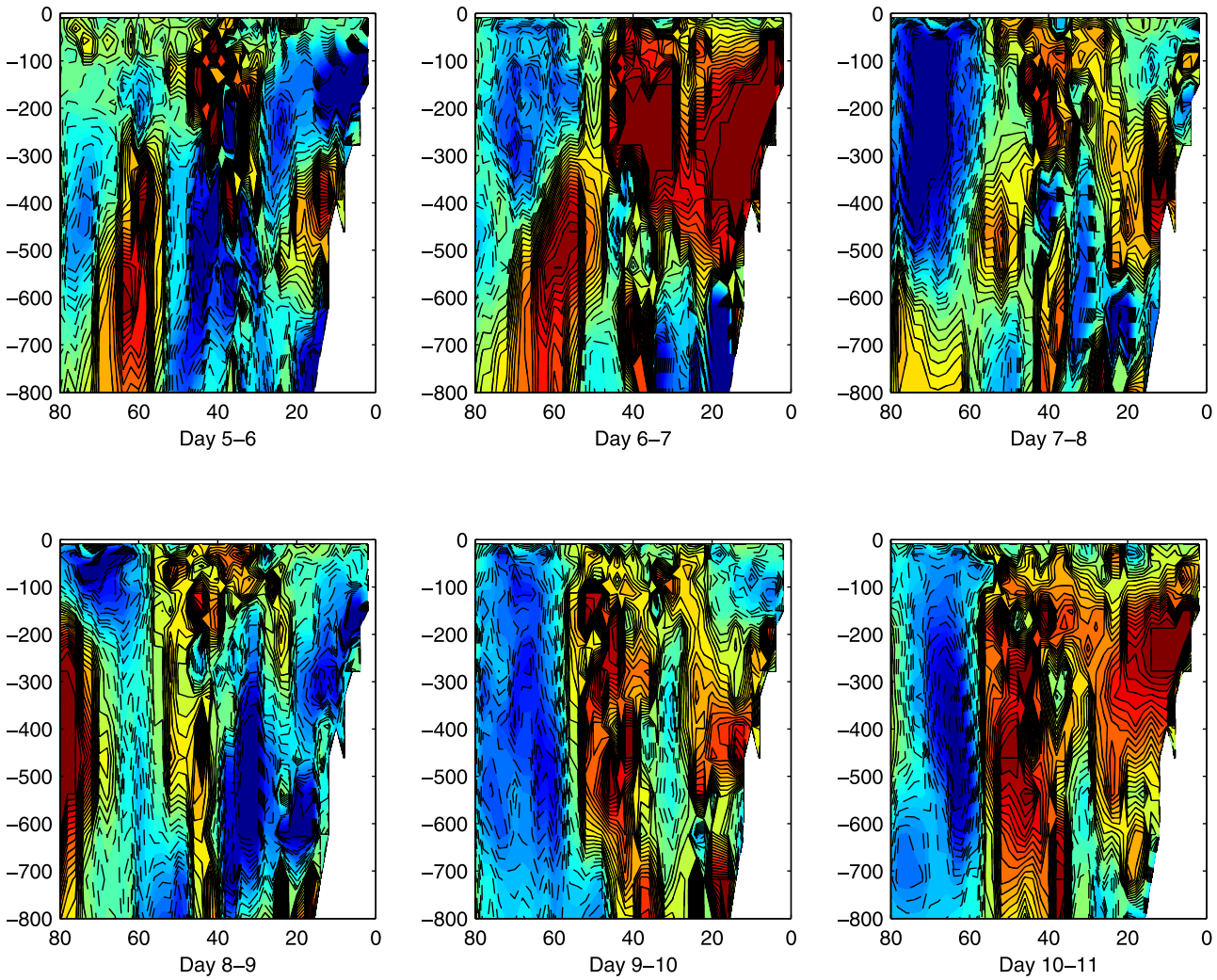

Figure 5. Contiguous daily averaged vertical velocity along the cross section through the center of MSC during spring upwelling starting from day 90 of year 8. Vertical velocities larger than 0.1 cm/s are marked as red while that smaller than −0.1 cm/s is marked as blue. Solid lines denote upward velocity while dash lines denote downward velocity. X-axis is the offshore distance (kilometers); y-axis is the depth (meters). The labeled day 0 corresponds to day 90 of year 8.

MSC. They depend on the strength and direction of the horizontal circulation and are also associated with larger downwelling offshore and local density inversions. According to *Shepard et al.* [1979], the tendency for up-canyon flow to occur more frequently than down-canyon flow in MSC is unique because the net flow in most submarine canyons is down-canyon. Local vertical overturning is also found inside MB and MSC. Note that downwelling occurs near the upstream rim of the canyon (Figure 2, depth ∼200 m). Downwelling in such regions is frequently observed [e.g., *Hickey*, 1997] during upwelling and is not well reproduced in sigma-coordinate numerical models [*Allen et al.*, 2003]. The overturning implies hydrostatic instabilities that lead to complex flow and enhanced mixing in this region. Our results show that MSC has a significant influence on the local circulation, including vertical transport, and thus enhanced turbulent mixing. In the next section, we further compare numerical simulations of Monterey Bay area with different depths of MSC.

[26] Figures 6–8 show the instantaneous horizontal temperature (Figures 6a, 7a, and 8a) and velocity fields (Figures 6b, 7b, and 8b) at depths of 10.1, 100, 200, and 400 m for 3 different days, 5 d apart, day 95, 100, and 105 of year 8 during a 10-d period in April. April is typically subject to the equatorward, upwelling-favorable winds in the California coast [*Hellerman and Rosenstein*, 1983]. Not only is vertical overturning important as shown previously in Figure 5 but horizontal advection contributes to mixing at all depths. It appears that the upwelled waters spread and mix at all depths due in part to the anticyclonic eddy and recirculation associated with the strong CUC. The CUC does not enter the bay itself but flows offshore beyond the bay and then divides into two branches near Point Año Nuevo (Figures 6–8, depth 200–400 m). The main branch continues to flow northward while the other branch becomes entrained in the local circulation inside the MSC, contributing to flow within the anticyclonic eddy. It is clear that the anticyclonic eddy significantly

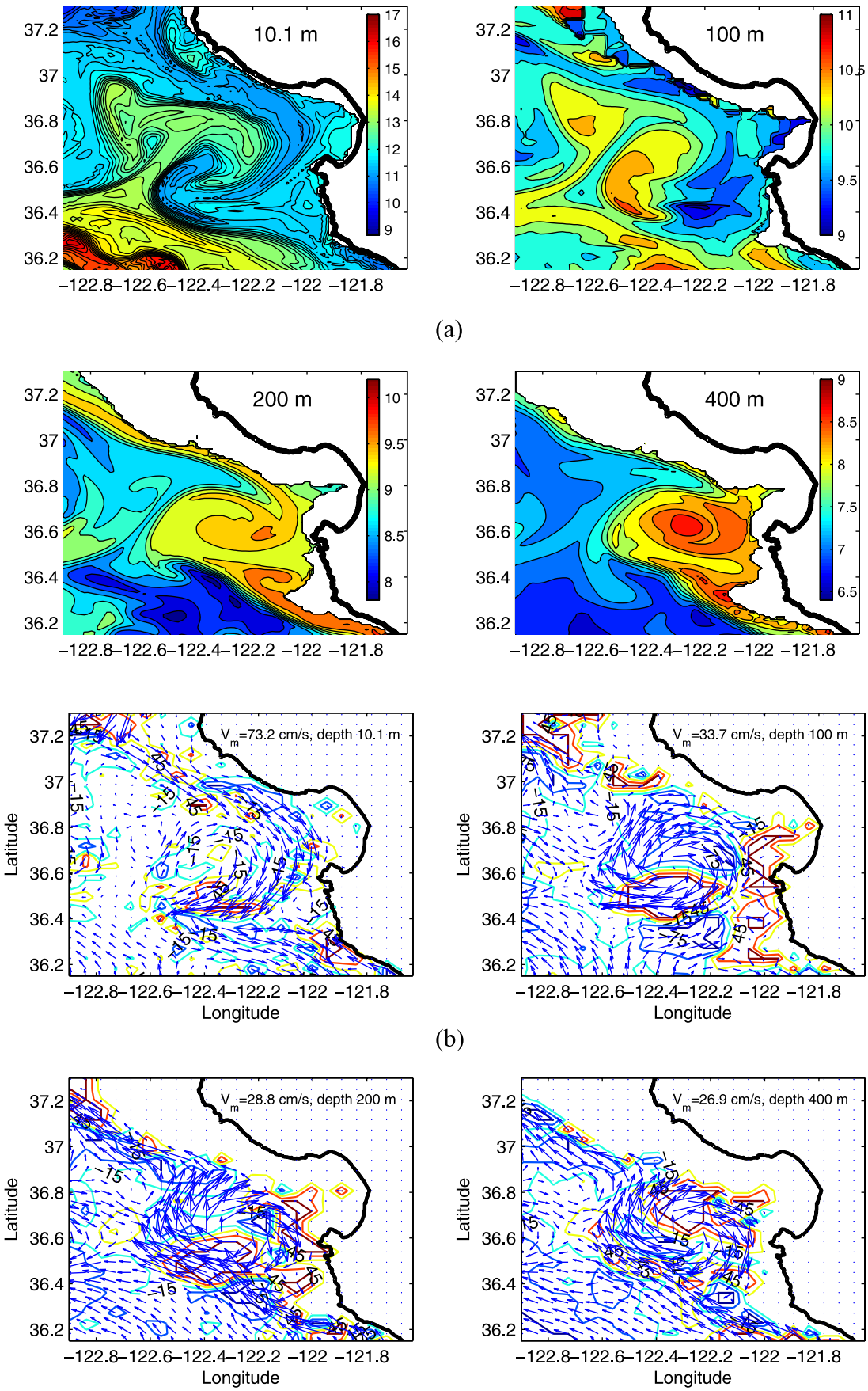

Figure 6. Instantaneous horizontal temperature and velocity fields at several depths on day 95 of year 8. Vertical velocity is represented by the contours.

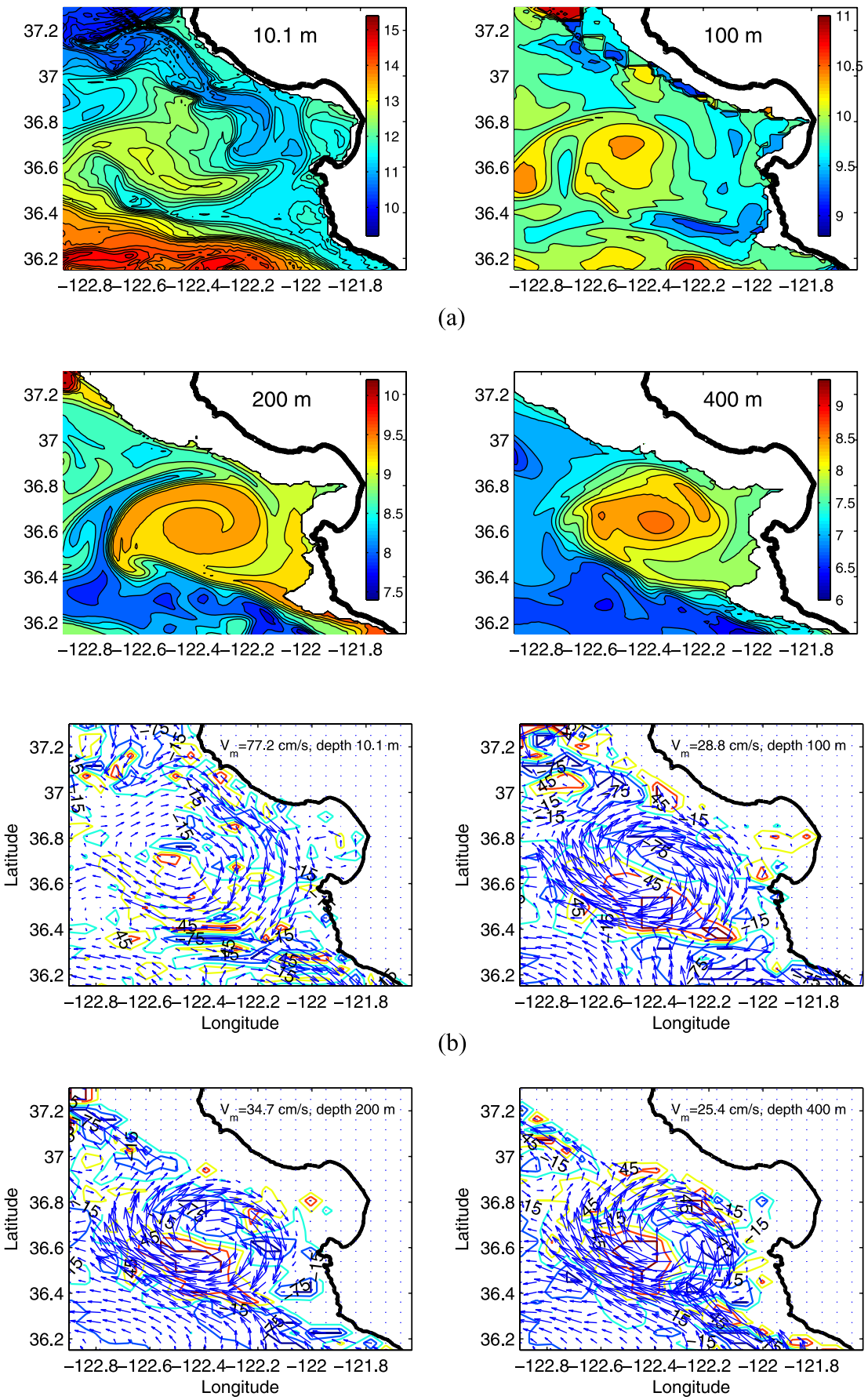

Figure 7. Same as Figure 6 on day 100 of year 8.

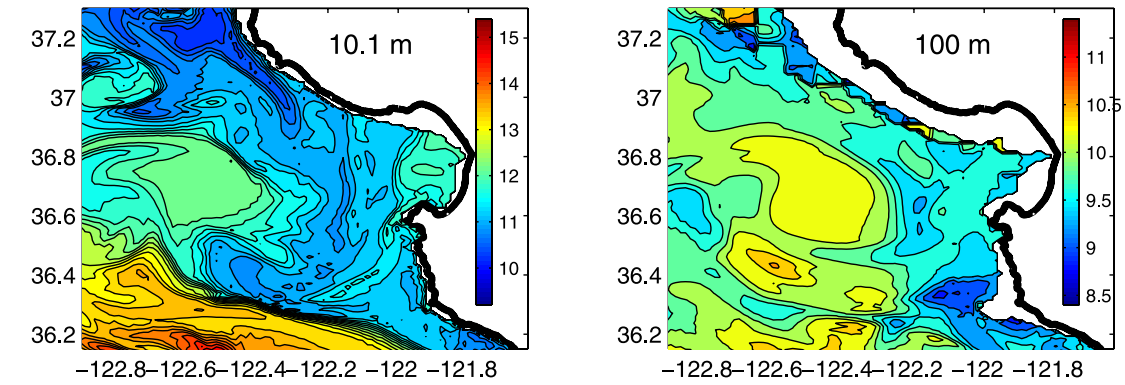

(a)

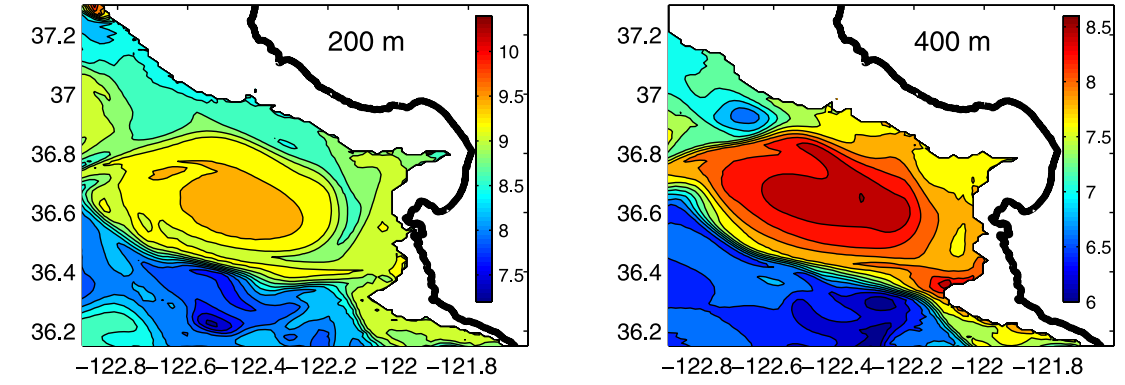

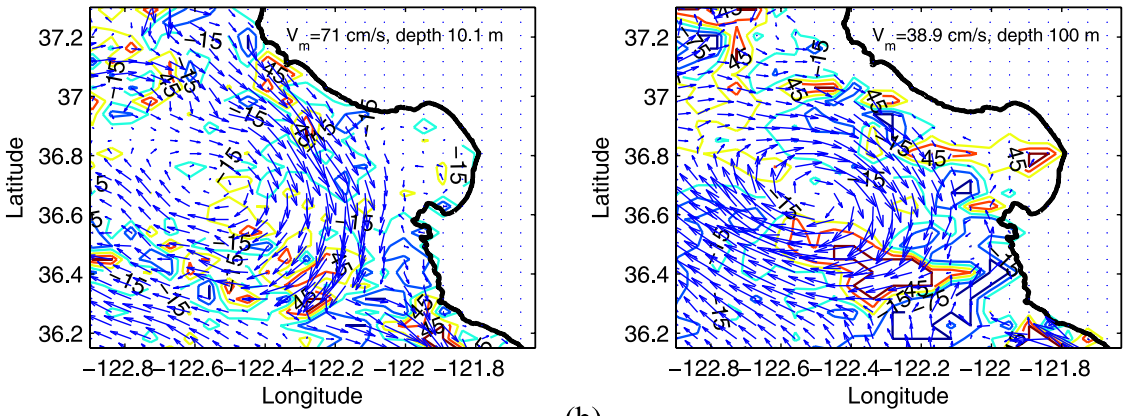

(b)

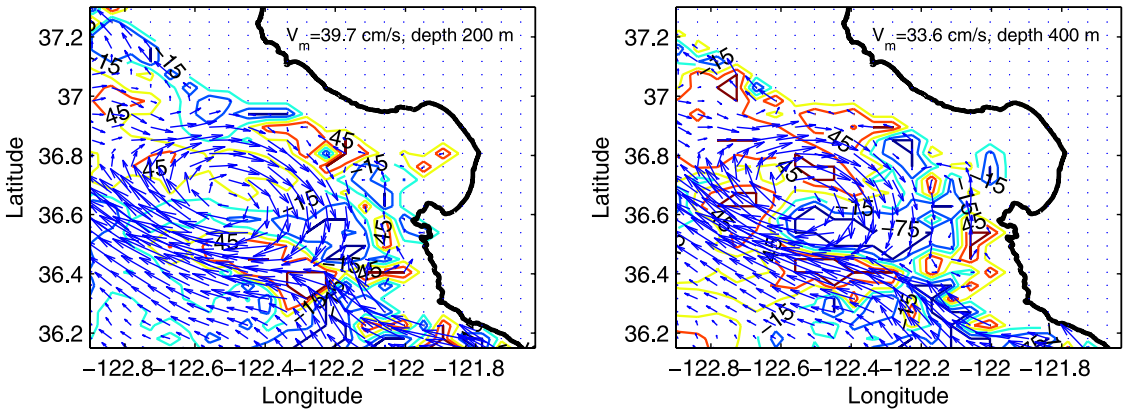

Figure 8. Same as Figure 6 on day 105 of year 8.

enhances the horizontal mixing. Apparently waters from the CUC that enter MB tend to follow the topography within the canyon up to certain levels but do not appear to reach the surface. These waters, constrained by stratification, most likely spread and mix horizontally before they ultimately reach the surface. Horizontal flow at deeper levels (Figures 6b, 7b, and 8b) further indicates that the waters entering MSC and upwelled to shallower levels primarily result from the CUC. The rise of deep waters within the canyon must also be due in part to bathymetric uplifting. These simulations of the deep circulation in MSC are consistent with earlier observations where the importance of bathymetrically induced upwelling was addressed [e.g., *Shepard*, 1975; *Breaker and Broenkow*, 1994].

[27] Weak correlation is expected between the local winds (within a day or so) and the currents observed in the vicinity of Monterey Bay. The currents established during upwelling-favorable winds are mainly forced by winds which are sustained for longer periods [*Ramp et al.*, 1997]. Both field observations and our simulations show that longer-period wind forcing is responsible for the generation of the currents as well as the meanders, eddies, and filament structures. During periods of sustained upwelling, the upwelling front continues to propagate offshore contributing to the growth of meanders and filaments, and the instabilities that develop are enhanced [*Tseng and Ferziger*, 2001; *Chao and Shaw*, 2002; *Tseng et al.*, 2005]. Short-term wind variations may have small-scale, local impacts which cannot be captured in our longer-term simulations. The influence of higher-resolution wind stress on shorter timescales will be investigated in a subsequent study.

[28] The simulations generate patterns of mesocale variability in SST, especially the highly visible cold filaments (Figure 4) during spring and summer, resembling the fields portrayed in satellite imagery [e.g., *Rosenfeld et al.*, 1994]. The temperature drop due to upwelling is approximately 3–4°C in the model, consistent with early observations [*Breaker and Broenkow*, 1994]. Our simulations also identify the source of cold surface water in MB that originates at Point Año Nuevo and bifurcates as it approaches the bay, providing dynamical support for the previous observations. On the basis of our simulation and early observation, an estimated volume transport of 0.2 Sv enters the bay based on a mean flow 20 cm/s. However, only 0.05 Sv is estimated to be upwelled from the canyon if assuming mean vertical velocity 0.1 cm/s (Figure 5). Most of the advected waters flow over the bay and/or flow offshore. The details are beyond the scope of this study.

[29] Forced by climatological winds, surface heating, and constrained by local topography, cyclonic and anticyclonic eddies form and evolve in the model domain. In Figure 7, for example, a surface filament develops and propagates westward during spring upwelling season, where the filament has grown to ~80 km in length and ~20 km wide. In Figure 8, another anticyclonic eddy is generated at the mouth of the Bay. Later, an eddy pinches off from the filament. These patterns and features are typical of the central California coast during strong equatorward, upwelling-favorable winds and add credibility to our model simulations and the forcing we have employed. Coastal capes often produce cold-core cyclonic eddies which often separate and move away from the coast. Both cyclonic and anticyclonic eddies are generated off Point Año Nuevo and Point Sur which serve as major upwelling centers just north and south of MB. Cyclonic eddies are more frequently observed off Point Sur because of topographic influences [*Traganza et al.*, 1983]. Finally, the smooth departure of the features from the model domain is reassuring and supports the one-way-nesting we have employed.

4. Effects of Monterey Submarine Canyon on the Circulation Within and Beyond the Bay

4.1. Impacts on the Circulation

[30] Capes along the coastline have been shown to be important for "anchoring" upwelling and filaments and enhancing the growth of meanders and eddies. Historically, MSC was thought to be responsible for strong upwelling of nutrient-rich water in the Monterey Bay [*Skogsberg*, 1936; *Skogsberg and Phelps*, 1946; *Bolin and Abbott*, 1963]. More recently, *Rosenfeld et al.* [1994] and *Breaker and Broenkow* [1994] questioned this interpretation. In recent years, several studies showed that the source of cold, salty, near-surface water in MB is primarily associated with the upwelling center at Point Año Nuevo rather than MSC itself [e.g., *Rosenfeld et al.*, 1994]. Cold, nutrient rich waters from this upwelling center are advected southward under the influence of the equatorward jet into the bay and offshore. Stratification isolates the upper water column from upward flow that originates deeper in the canyon. Our results support this view and further show that the upwelled waters from the deep canyon mix with the surrounding waters when they reach a certain depth (section 3.2) and that mixing is enhanced by the local topography. In this section, we try to gain a better understanding of how the complex topography associated with MSC influences the overlying circulation and physical properties during periods of upwelling.

[31] Figure 9 shows the monthly averaged horizontal velocities for April (Figure 9a) and November (Figure 9b) in cross-shore sections taken along the Canyon axis (Figure 1) at different depths. The black dots shown in Figure 9 correspond to the same dots in Figure 1. The near-surface currents respond to wind forcing with maximum equatorward flow in April having a jet-like structure, with maximum flow located 30–40 km offshore, while the near-surface flow is mainly to the northwest in November. In April, weak northward flow occurs inside the bay, producing the frequently observed cyclonic circulation near the surface (up to 20–30 km offshore). It is clear that the strongest equatorward flow in April is restricted to the upper 50 m or so but occasionally reaches deeper levels. The flow direction changes poleward around 50–200 m depth. The anticyclonic eddy is observed just outside the mouth of Monterey Bay from intermediate depths to depths of 600 m or deeper. The poleward undercurrent is well developed beneath the equatorward jet near the coast. The undercurrent flows across the mouth of Monterey Bay and appears to be continuous in the offshore direction out to at least 80 km from the coast. The poleward undercurrent, although well-defined, is relatively weak (~5 cm/s) during the early part of a year, but intensifies in the fall and winter and becomes indistinguishable from the DC (Figure 5). The nearshore,

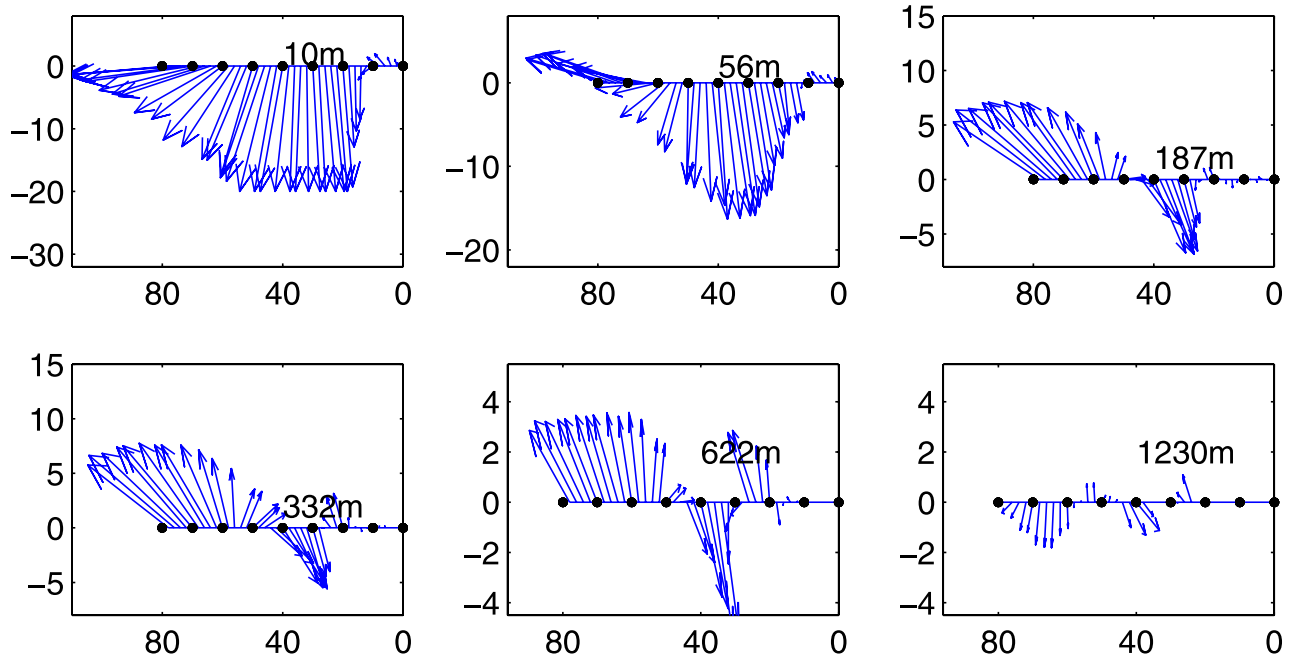

(a) Monthly averaged velocity vector in April

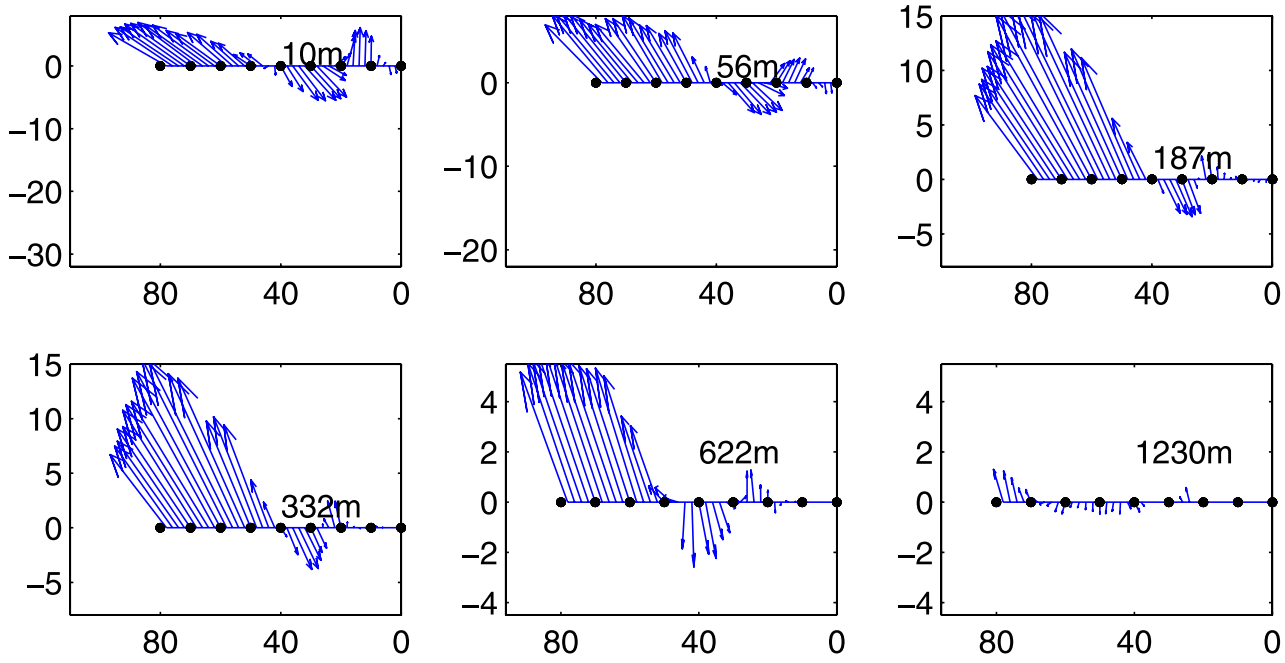

(b) Monthly averaged velocity vector in November

Figure 9. The monthly averaged (taken from year 8) horizontal velocity vector in a cross-shore section cut through the center of MSC (the dash lines in Figure 1) at different depths during (a) April and (b) November. X-axis is offshore distance (kilometers). The unit in Y-axis is cm/s.

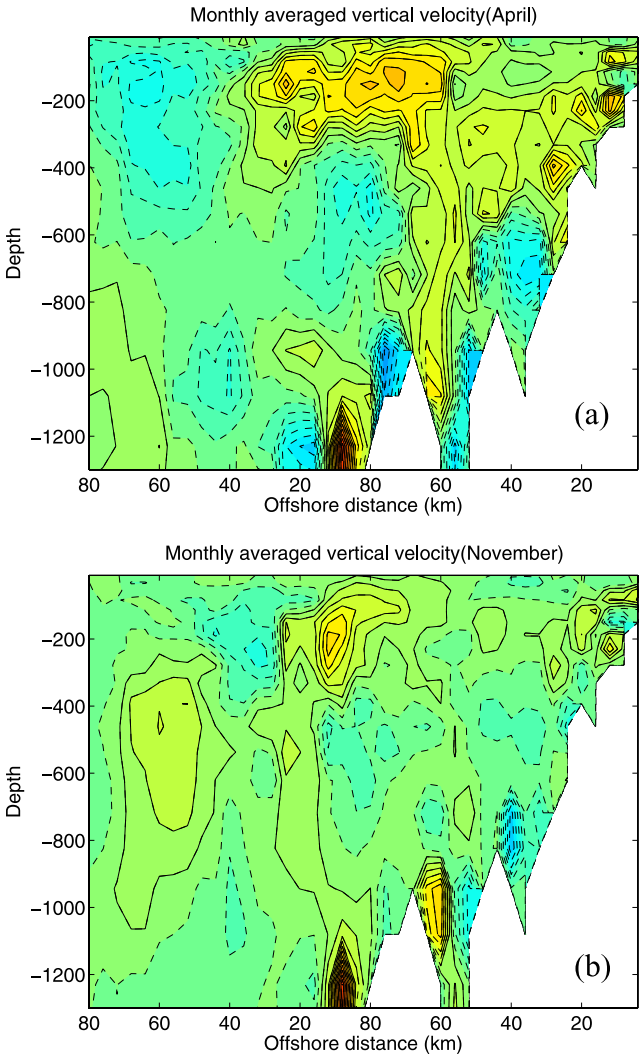

Figure 10. The monthly averaged vertical velocity contours in a cross-shore section cut through the center of MSC (the dashed lines in Figure 1) at different depths (April in year 8) during (a) April and (b) November. The contours range from −0.02 cm/s to 0.02 cm/s. Solid lines denote upward velocity while dash lines denote downward velocity.

equatorward jet has maximum mean speeds of ∼25 cm/s, and the poleward undercurrent has maximum mean speeds of 5–10 cm/s at depths of 100–500 m. These values are in good agreement with past observations [*Collins et al.*, 2000; *Ramp et al.*, 1997; *Paduan and Rosenfeld*, 1996].

[32] Several features are noteworthy. First, the offshore anticyclonic eddy occurs at depths from 187 m to at least 600 m in both months and, presumably, year-round. Second, the mean surface circulation within the bay is cyclonic in April while the circulation is mainly anticyclonic in November. Third, the CUC is evident along the coast in both months but is stronger in November. There is a westward/offshore component to flow in the CUC at all depths. This feature has been observed before and is mainly due to bathymetric influences and Rossby wave propagation [*Ramp et al.*, 1997]. We also observe anticyclonic circulation inside MSC described in section 3.

[33] Figure 10 shows the monthly averaged temperatures (Figure 10a) and vertical velocities (Figure 10b) for the vertical-section along the Canyon axis for April. The effects of stratification are clearly seen. The topography also affects the stratification at deeper levels. MSC is responsible for recirculation and larger vertical velocity variations inside the bay at depth (up to 35 km offshore). Vertical velocities with larger magnitudes often occur near the canyon bottom, consistent with the results of *Breaker and Broenkow* [1994]. Strong surface upwelling near the mouth of Monterey Bay also occurs, which may be associated with the upwelled waters that are advected southward from Point Año Nuevo. The strong vertical velocities show that the currents near the canyon head tend to follow the canyon topography. The downward vertical motion, just inside the canyon rim, is consistent with observations of isopycnals over Astoria Canyon [*Hickey*, 1997]. Also, the stratification in the upper 200 m is only marginally stable. Cold waters from intermediate depths (∼100–200 m) rise toward the surface near the mouth of the Bay with downward motion observed beyond and below the region of subsurface maxima in upward motion. Finally, the near-surface and deep circulations appear to be unrelated.

4.2. Impact of Monterey Submarine Canyon on the Circulation

[34] The influence of MSC may have a significant impact on the local circulation due to its size and steep topography. The effect of MSC on the circulation in Monterey Bay has been examined on at least one occasion by *Bruner* [1988], and his work also motivates us to revisit this question. *Bruner* [1988] used a simple, two-layer model to determine the effects of bottom topography, inflow and outflow location and magnitude, and vertical shear. The model domain covered only the bay itself with 1.8 km resolution, and wind forcing and bottom friction were not included. In three experiments, the bottom topography associated with MSC was removed by replacing a flat bottom at a depth of 750 m, and in the other four experiments, the canyon was retained. His results showed that, when the deep canyon became shallower, flow in the lower layer tended to follow the boundaries of the bay instead of the topography itself, and had little effect on the upper layer. Vertical shear between the two layers was found to be important for the barotropic case where the flow magnitudes in each layer were similar, resulting in circulation at the surface resembling the flow in the lower layer. In order to examine the impact of the canyon on the circulation in the vicinity of Monterey Bay, we have performed additional nonhydrostatic simulations with all boundary conditions and boundary forcing refrained as before except for the bottom boundary. Similar to *Bruner* [1988], the deep canyon was filled to three different depths such that the maximum depth was first set at 880 m, and then more filling was added such that the maximum depth was next 580 m, and finally it was filled such that the maximum depth was 300 m. The bathymetry for the three stage depth removal is illustrated by the bold lines shown in Figure 1. Gradual depth removal in MSC can better help us to explain the source of the upwelling water discussed in section 3.2, and to observe the

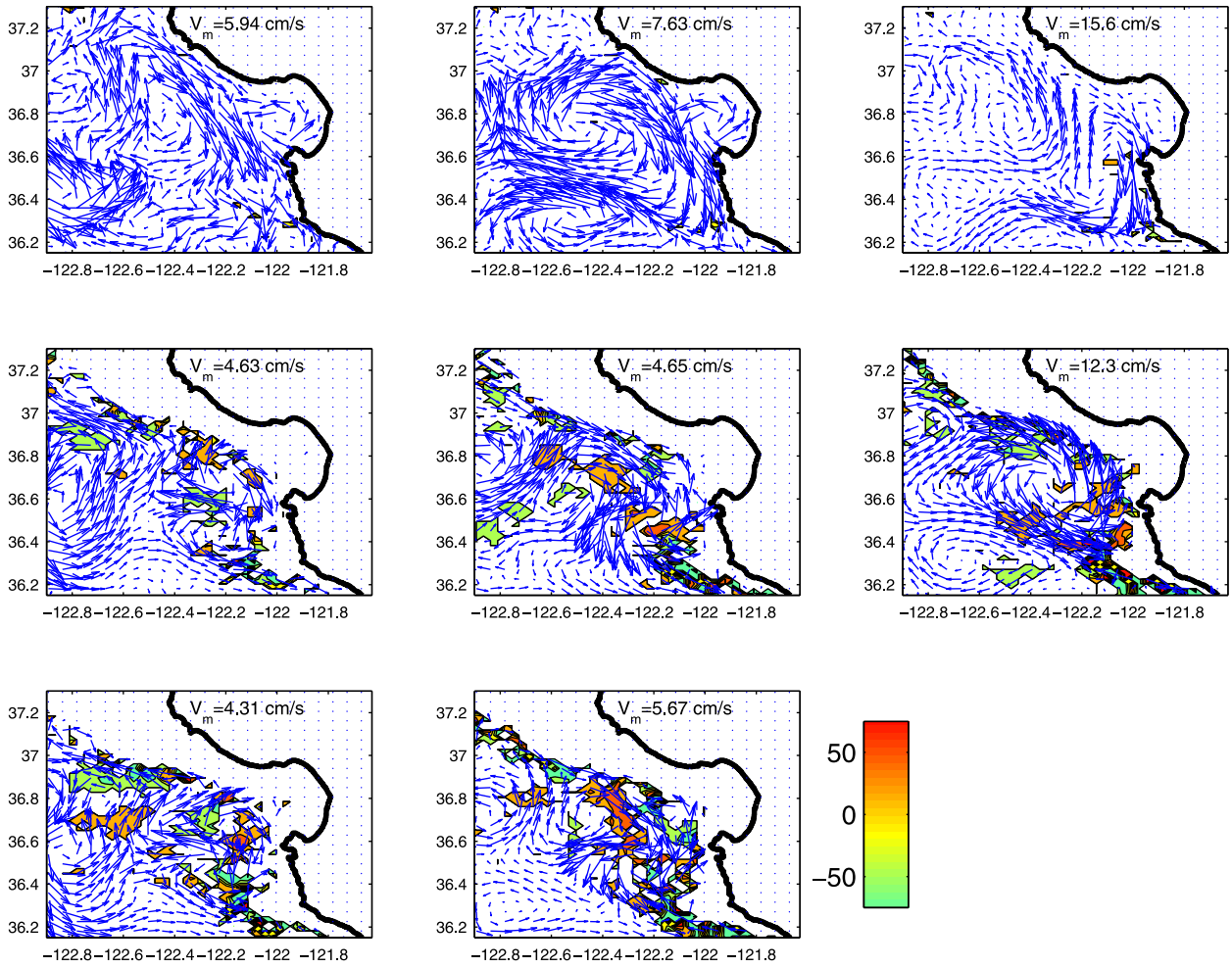

Figure 11. The mean velocity difference between the cases "filling MSC" and "not-filling MSC" ($V_d = V_{\text{filling MSC}} - V_{\text{not-filling MSC}}$) during summer (May to August) at depth (top) 10.1 m, (middle) 200 m, and (bottom) 400 m. The topography is replaced by a flat bottom at 880 m, 580 m, and 300 m (from left to right), respectively. V_m denotes the maximum velocity difference. The color contours mark the absolute magnitude of vertical velocity greater than 5 m/week. The unit of vertical velocity in the color bar is meters/week.

gradual influence of the MSC in the horizontal circulation as the canyon becomes shallower.

[35] Figure 11 shows comparisons of the mean velocity differences between the cases "filling" and "not-filling" MSC ($V_d = V_{\text{filling MSC}} - V_{\text{not-filling MSC}}$) during summer (May to August) at depths of 10.1 m (top), 200 m (middle), and 400 m (bottom). As indicated, the topography has been replaced by a flat bottom at 880 m, 580 m, and 300 m (from left to right), respectively. V_m represents the maximum velocity difference which is less than 20% of the maximum mean horizontal velocities shown in Figures 2–3. The color contours mark the magnitude of vertical velocity differences greater than ±5 cm/s. Figure 12 shows the same comparison during winter (November to February). A stronger cyclonic (anticyclonic) eddy is observed inside the Bay in summer (winter) when MSC is filled, indicating that the circulation inside the Bay is further constrained by the topography. Differences in the eddy fields are also observed above MSC, Sur Ridge and other areas. Larger differences are observed in summer rather than in winter (see Figures 11 and 12, right). Surface flow near the Monterey peninsula changes direction as the MSC is further filled (Figure 11). A pair of cyclonic and anticyclonic eddies is also formed at the mouth of Monterey Bay at depth. The deep circulation inside Monterey Bay is consistent with the conceptual flow diagram of *Breaker and Broenkow* [1994]. At 200 m, the anticyclonic circulation outside Monterey Bay appears weaker in the third case where MSC is filled to a depth of 300 m (Figures 11–12, right). These differences are directly associated with the local topography. The larger-scale circulation is dominated by the CCS through the open boundaries, while the eddies are subject to the influence of the local bathymetry. The differences in vertical velocity are larger at 200 m and 400 m; larger vertical motions are observed deeper in MSC (~200–400 m) as the false bottom gets shallower. This is evident in MSC and Sur Ridge. In particular, larger downwelling occurs when MSC is removed. Overall, we see that the presence of the canyon has a major impact on vertical motion and that it is not restricted to the canyon itself.

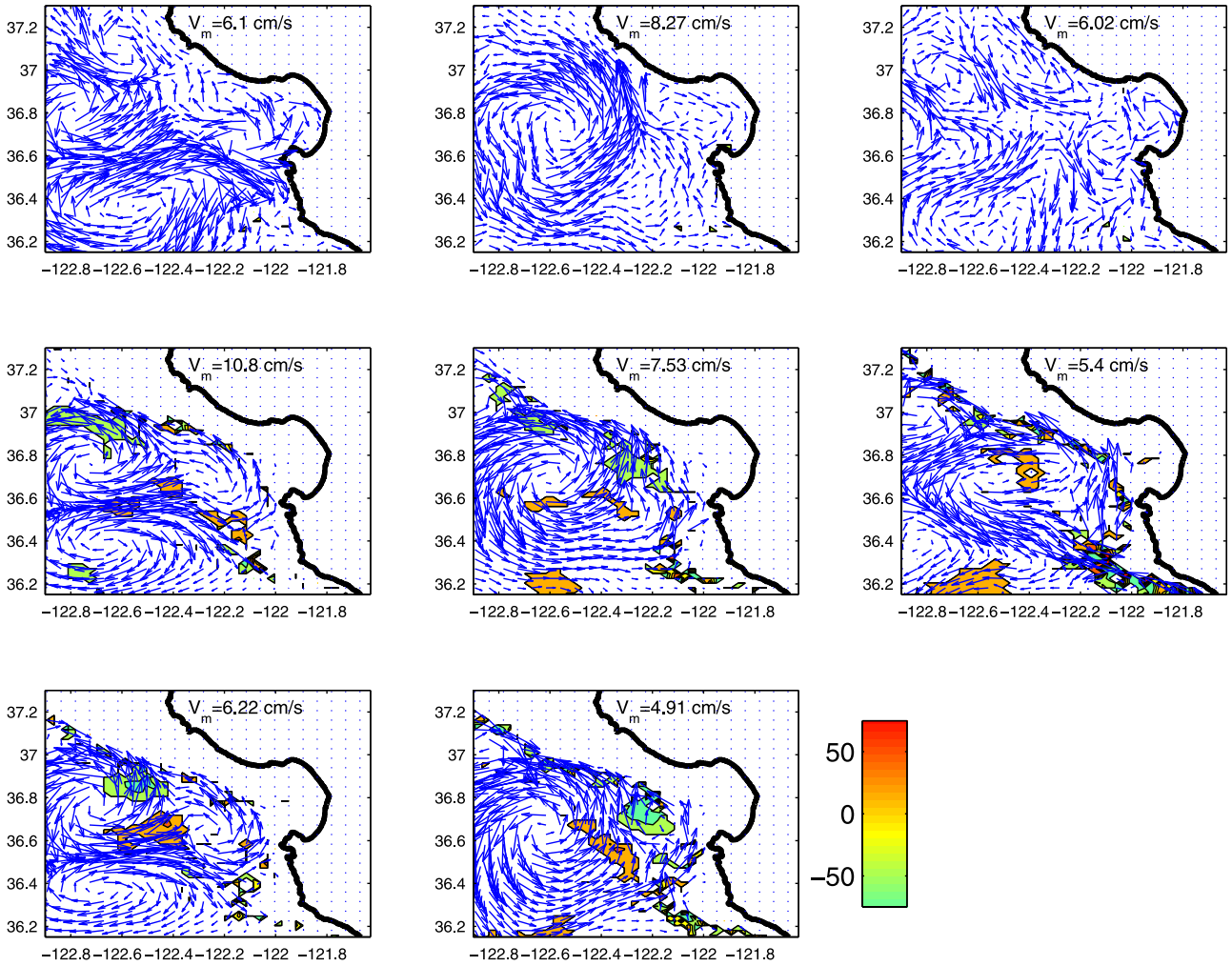

Figure 12. Same as Figure 11 during winter (November to February).

[36] Figures 13 and 14 show a comparison of mean kinetic energy differences "filling" and "not-filling" the MSC during summer and winter, respectively. The deep canyon is filled at 880 m (left) and 580 m (right) for the cases filling the MSC. In the absence of the MSC, the kinetic energy field is stronger overall just above the deep canyon. Higher kinetic energy is also observed in other years during the same period. A band of high energy extends further northwestward into the Canyon in the presence of MSC and is associated with a low-energy area offshore. The vorticity in this region appears to be dominated by the shearing stresses associated with this feature. Over the canyon and along the slopes, the tendency toward cyclonic rotation is almost certainly due to vortex stretching over the steep topography. The areas of strong kinetic energy along the continental slopes and across the canyon tend to follow the boundaries.

[37] Finally, we compare the circulation of Monterey Bay based on the results of *Rosenfeld et al.* [1994] and *Breaker and Broenkow* [1994] with model simulations obtained in this study. Figure 15 shows monthly averaged vertical sections for the latitudinal ("*v*") component of velocity from the surface to 1400 m along the axis of MSC (Figure 1), for April and November. The pattern of bifurcated flow as described by *Rosenfeld et al.* [1994] is readily observed in the vertical section for April with strong surface flow to the south centered at 40 km offshore, and weak northward flow near the surface inside the bay, and strong northward flow from 60 to 80 km offshore, centered at a depth of 300 m. The model results show that southward flow associated with the equatorward jet clearly separates northward flow inside the bay from northward flow outside the bay, and that northward flow inside the bay is small compared to the northward flow associated with the western half of the anticyclonic eddy offshore. In November, flow to the south has weakened significantly, but northward flow inside and outside the bay has intensified, consistent with the arrival of the DC and seasonally intensified flow in the CUC.

[38] On the basis of a conceptual model of the circulation in Monterey Bay, *Breaker and Broenkow* [1994] indicated that circulation might consist of three layers, a surface layer extending to a depth of about 30 m, a second layer between roughly 30 and 250 m, and a third layer from roughly 250 m, to the bottom. Both vertical sections indicate a shallow surface layer inside bay extending to depths of at least 50 m, and a second layer centered at depths of 300–400 m. Further offshore, even a third layer may be indicated at

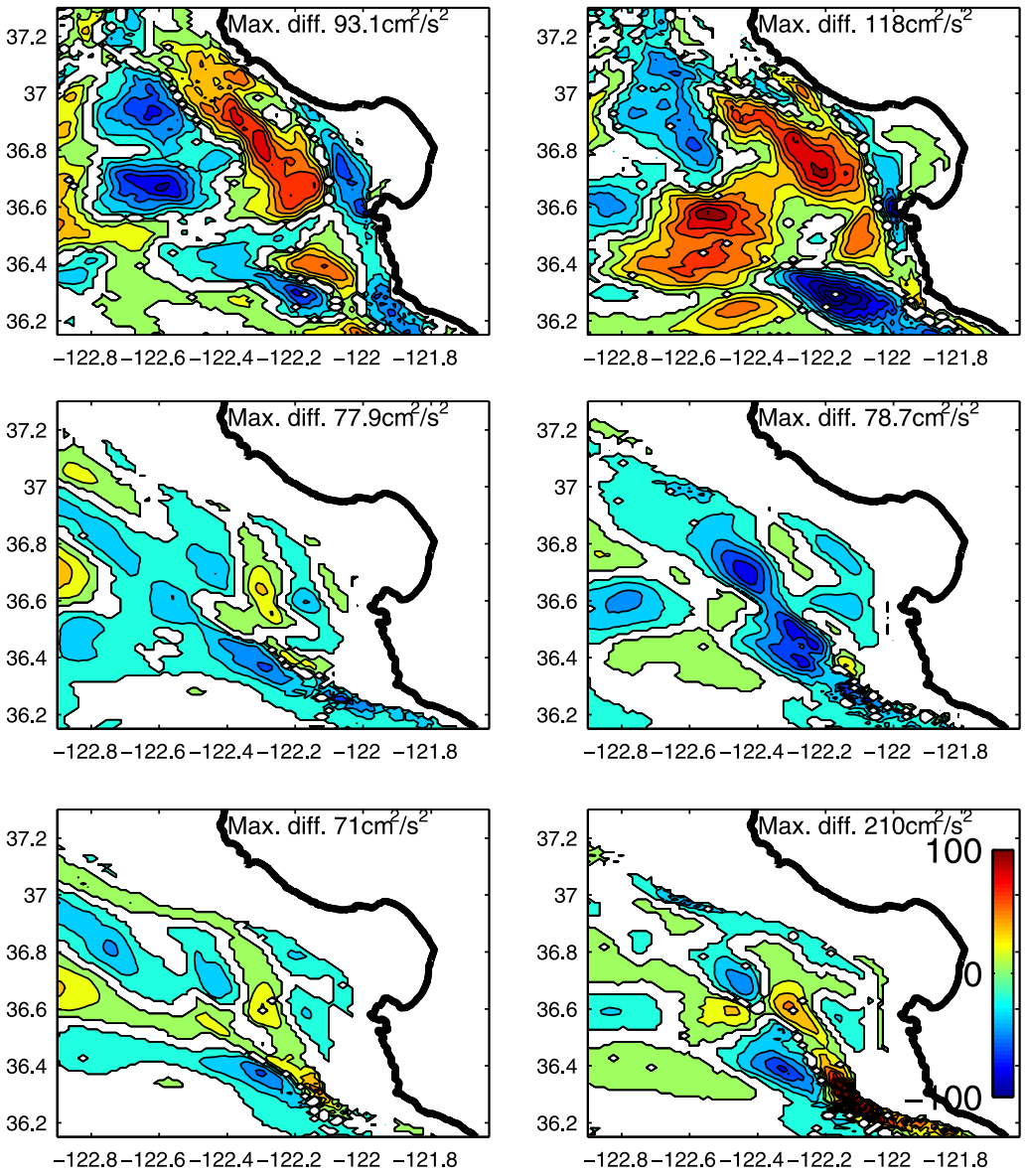

Figure 13. Comparison of the total kinetic energy difference between the cases "filling" and "not-filling" MSC during summer at depth (top) 10.1 m, (middle) 200 m, and (bottom) 400 m. The topography is replaced by a flat bottom at (left) 880 m and (right) 580 m, respectively. The color contours mark the absolute magnitude greater than 5 cm^2/s^2. The color bar has unit cm^2/s^2.

depths of 1000 m or greater. Thus there may be agreement with Breaker and Broenkow's conceptual model concerning the number of layers but less agreement on the thickness of each layer. Further investigation is required.

5. Summary

[39] The high resolution, nonhydrostatic Monterey Bay area regional model was used to investigate the regional circulation and the effects of Monterey Submarine Caynon. The model is coupled to a larger-scale CCS model to include dynamics from the open ocean. The Monterey Bay area circulation is highly correlated with the CCS. The flow patterns in summer are significantly different from those in winter. Within the bay weak cyclonic circulation is often observed. This feature is a result of the coastal geometry and the bifurcated flow from Point Año Nuevo. A warm anticyclone is often seen just offshore of Monterey Bay at depth year-round, a feature which is strongly influenced by topographic effects and is better developed during winter. We investigated the effect of MSC on flow during the upwelling season, during which the surface equatorward flow dominates. Our results also indicate that CUC (200–400 m) does not enter the bay itself but swings offshore near Point Sur where it appears to separate from the coast and reform further north of the Bay. The CUC also appears to contribute to the anticyclonic circulation associated with the eddy through torque provided by larger horizontal shears near the western boundary of this feature. Vertical motions are also found greater during summer. They are mostly pronounced at depths of 50–200 m. The deep waters inside MSC are upwelled and then spread along

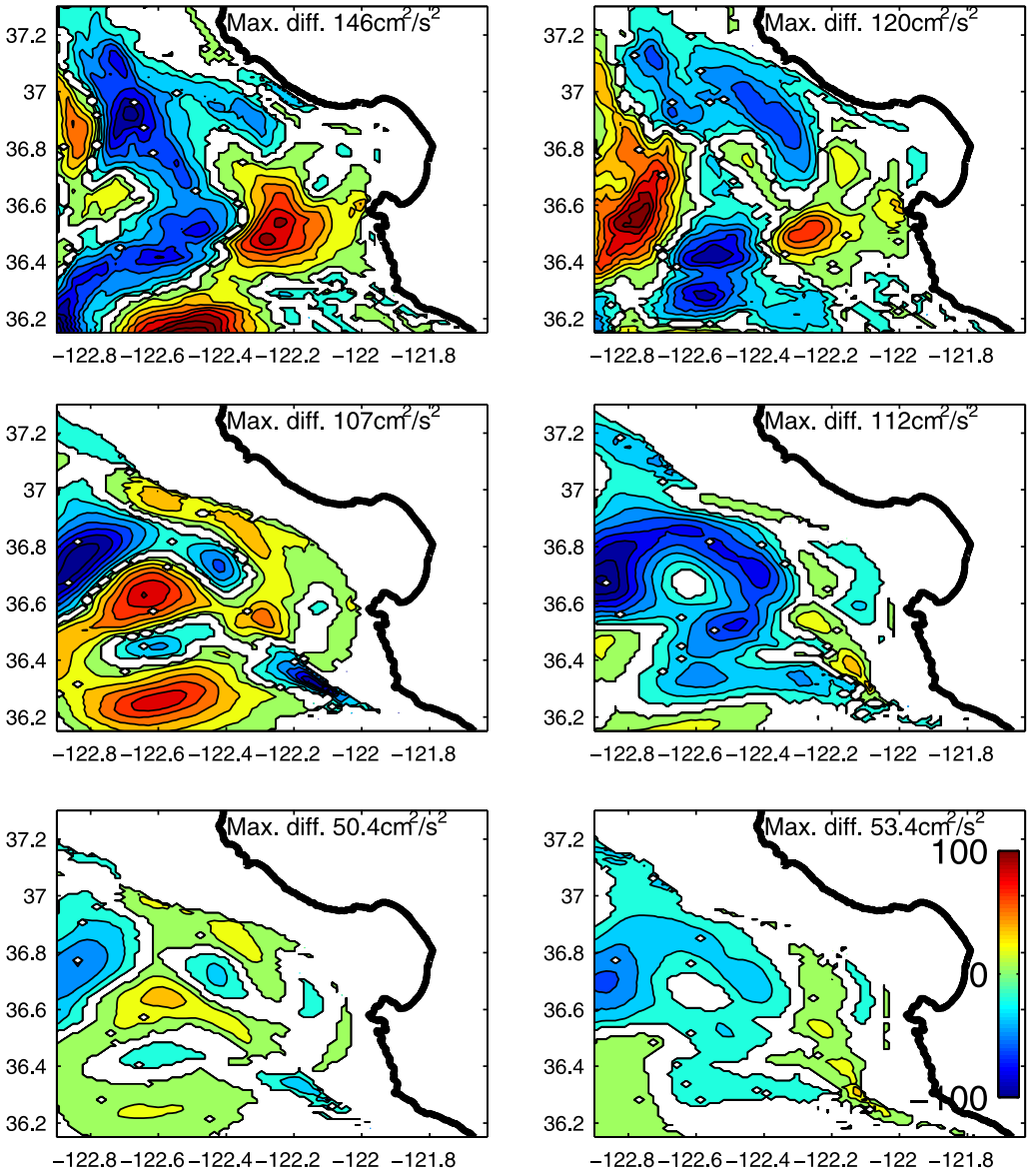

Figure 14. Same as Figure 13 during winter.

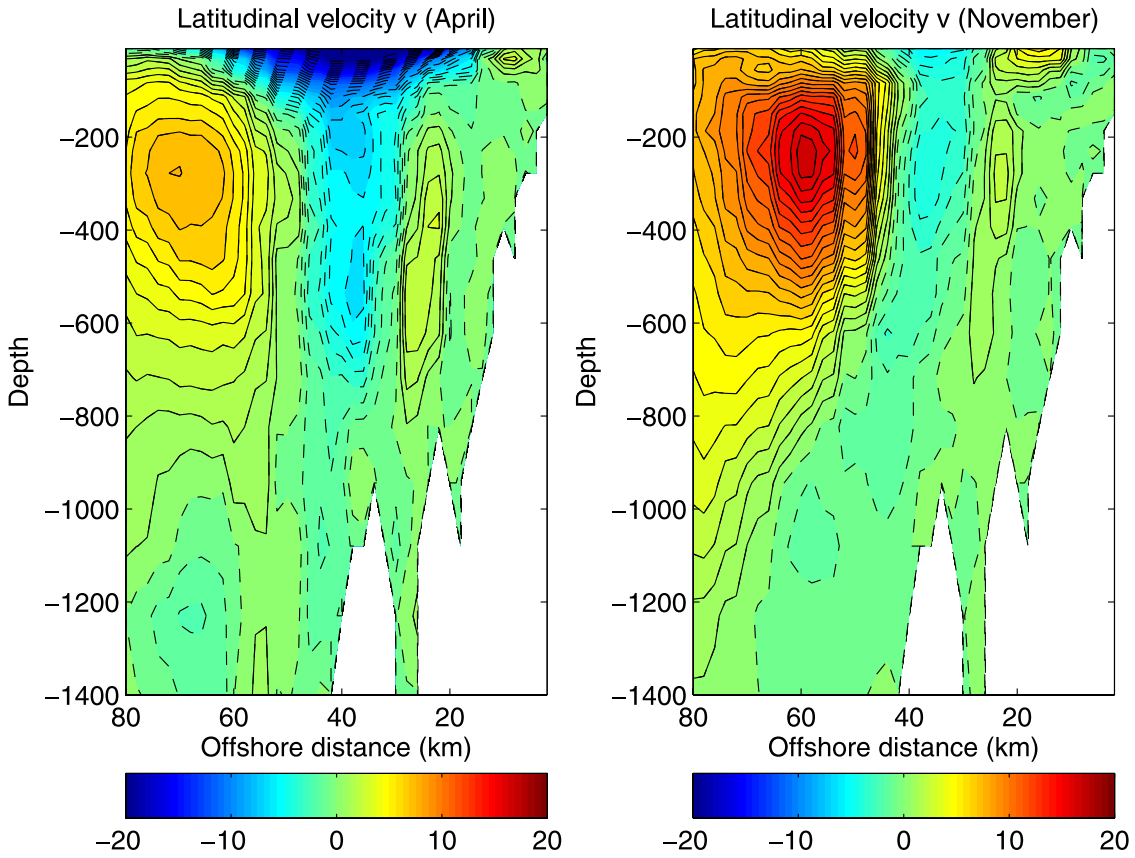

Figure 15. Comparison of the monthly averaged vertical sections in April and November for the latitudinal ("*v*") component of velocity from the surface to 1400 m along the axis of MSC (see Figure 1).

the canyon wall quickly before they reach the surface. Vortex stretching over the canyon just beyond the entrance to Monterey Bay, and along the adjacent continental slopes, in both cases, contributes to cyclonic circulation at deeper levels. Vertical sections of velocity along the axis of MSC indicate horizontal and vertical patterns of flow that are generally consistent with past observations on the circulation of Monterey Bay.

[40] **Acknowledgments.** Financial support from National Science Council, Taiwan (grant NSC 952119M002048) is appreciated. Useful suggestions and comments from the associate editor and anonymous reviewers are gratefully acknowledged. We are grateful to the National Center for High-Performance Computing, Taiwan, for computer time and facilities.

References

Allen, S. E., M. S. Dinniman, J. M. Klinck, D. D. Gorby, A. J. Hewett, and B. M. Hickey (2003), On vertical advection truncation errors in terrain-following numerical models: Comparison to a laboratory model for upwelling over submarine canyons, *J. Geophys. Res.*, *108*(C1), 3003, doi:10.1029/2001JC000978.

Bolin, R. L., and D. P. Abbott (1963), Studies on the marine climate and phytoplankton of the central coastal area of California, 1954–1960, *Calif. Coop. Oceanic Fish. Invest.*, *9*, 23–45.

Breaker, L. C. (2005), What's happening in Monterey Bay on seasonal to interdecadal time scales?, *Cont. Shelf Res.*, *25*, 1159–1193.

Breaker, L. C., and W. Broenkow (1994), The circulation of Monterey Bay and related processes, *Oceanogr. Mar. Biol.*, *32*, 1–64.

Breaker, L. C., and C. N. K. Mooers (1986), Oceanic variability off the central California coast, *Progr. Oceanogr.*, *17*, 61–135.

Bruner, B. L. (1988), A numerical study of baroclinic circulation in Monterey Bay, M. S. thesis, Naval Postgrad. Sch., Monterey, Calif.

Chao, S. Y., and P. T. Shaw (2002), Nonhydrostatic aspects of coastal upwelling meanders and filaments off eastern ocean boundaries, *Tellus, Ser. A*, *54*, 63–75.

Collins, C. A., N. Garfield, T. A. Rago, F. W. Rischmiller, and E. Carter (2000), Mean structure of the inshore countercurrent and California Undercurrent off Point Sur, California, *Deep Sea Res.*, *47*, 765–782.

Dietrich, D. E. (1997), Application of a modified "a" grid ocean model having reduced numerical dispersion to the Gulf of Mexico circulation, *Dyn. Atmos. Oceans*, *27*, 201–217.

Dietrich, D. E., and C. A. Lin (2002), Effects of hydrostatic approximation and resolution on the simulation of convective adjustment, *Tellus, Ser. A*, *54*, 34–43.

Dietrich, D. E., A. Mehra, R. L. Haney, M. J. Bowman, and Y. H. Tseng (2004), Dissipation effects in north Atlantic ocean modeling, *Geophys. Res. Lett.*, *31*, L05302 doi:10.1029/2003GL019015.

Dukowicz, J. K., R. D. Smith, and R. C. Malone (1993), A reformulation and implementation of the Bryan-Cox-Semtner Ocean model on the connection machine, *J. Atmos. Oceanic Technol.*, *10*, 195–208.

Fringer, O. B., and R. L. Street (2003), The dynamics of breaking progressive interfacial waves, *J. Fluid Mech.*, *494*, 319–353.

Haney, R. L. (1991), On the pressure gradient force over steep topography in sigma coordinate ocean models, *J. Phys. Oceanogr.*, *21*, 610–619.

Haney, R. L., R. A. Hale, and D. E. Dietrich (2001), Offshore propagation of eddy kinetic energy in the California Current, *J. Geophys. Res.*, *106*, 11,709–11,717.

Hellerman, S., and M. Rosenstein (1983), Normal monthly wind stress over the world ocean with error estimates, *J. Phys. Oceanogr.*, *13*, 1093–1104.

Hickey, B. M. (1979), The California Current System: Hypotheses and facts, *Progr. Oceanogr.*, *8*, 191–279.

Hickey, B. M. (1997), The response of a steep-sided, narrow canyon to time variable wind forcing, *J. Phys. Oceanogr.*, *27*, 697–726.

Hodges, B. R., B. Laval, and B. M. Wadzuk (2006), Numerical error assessment and a temporal horizon for internal waves in a hydrostatic model, *Ocean Model.*, *108*, 44–64.

Jachec, S. M., O. B. Fringer, M. G. Gerritsen, and R. L. Street (2006), Numerical simulation of internal tides and the resulting energetics within Monterey Bay and the surrounding area, *Geophys. Res. Lett.*, *33*, L12605, doi:10.1029/2006GL026314.

Jan, S., D. E. Dietrich, Y. H. Tseng, and Y. Yang (2006), Development of a low-dissipation, high-computational-efficiency duo-grid Pacific Ocean model (DUPOM), *Eos Trans. AGU*, *87*(36), Ocean Sci. Meet. Suppl., Abstract OS46F-15.

Klinck, J. M. (1996), Circulation near submarine canyons: A modeling study, *J. Geophys. Res.*, *101*, 1211–1223.

Levitus, S. (1982), Climatological atlas of the world oceans, *NOAA Prof. Pap. 13*, 173 pp., U. S. Govt. Print. Off., Washington, D. C.

Li, Z., Y. Chao, X. Wang, J. Farrara, J. C. McWilliams, and K. Ide (2006), Implementation of a three-dimensional variational data assimilation for ROMS real-time forecasting, *Eos Trans. AGU*, *87*(36), Ocean Sci. Meet. Suppl., Abstract OS26O–15.

Ly, L. N., and P. A. Luong (1999), Numerical grid used in a coastal ocean model with breaking wave effects, *J. Comput. Appl. Math.*, *103*, 125–137.

Mooers, C. N. K., C. A. Collins, and R. L. Smith (1976), The dynamics structure of the frontal zone in the coastal upwelling region off Oregon, *J. Phys. Oceanogr.*, *6*, 3–21.

Narimousa, S., and T. Maxworthy (1989), Application of a laboratory model to the interpretation of satellite and field observations, *Dyn. Atmos. Oceans*, *13*, 1–46.

Pacanowski, R. C., and S. G. H. Philander (1981), Parameterization of vertical mixing in numerical models of tropical oceans, *J. Phys. Oceanogr.*, *11*, 1443–1451.

Paduan, J. D., and L. K. Rosenfeld (1996), Remotely sensed surface currents in Monterey Bay from shore-based HF radar (CODAR), *J. Geophys. Res.*, *101*, 20,669–20,686.

Paduan, J. D., and I. Shulman (2004), HF radar data assimilation in the Monterey Bay area, *J. Geophys. Res.*, *109*, C07S09, doi:10.1029/2003JC001949.

Penven, P., L. Debreu, P. Marchesiello, and J. C. McWilliams (2006), Evaluation and application of the ROMS 1-way embedding procedure to the central California upwelling system, *Ocean Model.*, *12*, 157–187.

Petruncio, E. T., J. D. Paduan, and L. K. Rosenfeld (2002), Numerical simulations of the internal tide in a submarine canyon, *Ocean Model.*, *4*, 221–248.

Pickett, M. H., and J. D. Paduan (2003), Ekman transport and pumping in the California Current based on the U. S. Navy's high-resolution atmospheric model (COAMPS), *J. Geophys. Res.*, *108*(C10), 3327, doi:10.1029/2003JC001902.

Ramp, S. R., L. K. Rosenfeld, T. D. Tisch, and M. R. Hicks (1997), Moored observations of the current and temperature structure over the continental slope off central California: 1. A basic description of the variability, *J. Geophy. Res.*, *102*, 22,877–22,902.

Rosenfeld, L. K., F. B. Schwing, N. Garfield, and D. E. Tracy (1994), Bifurcated flow from an upwelling center–a cold-water source for Monterey Bay, *Cont. Shelf Res.*, *14*, 931–964.

She, J., and J. M. Klinck (2000), Flow near submarine canyons driven by constant winds, *J. Geophys. Res.*, *105*, 28,671–28,694.

Shepard, F. P. (1975), Progress of internal waves along submarine canyon, *Mar. Geol.*, *19*, 131–138.

Shepard, F. P., N. F. Marshall, P. A. McLoughlin, and G. G. Sullivan (1979), Currents in submarine canyons and other sea valleys, *AAPG Studies in Geology*, vol. 8, pp. 1–13, Am. Assoc. of Petrol. Geol., Tulsa, Okla.

Shulman, I., C. R. Wu, J. K. Lewis, J. D. Paduan, L. K. Rosenfeld, J. C. Kindle, S. R. Ramp, and C. A. Collins (2002), High resolution modeling and data assimilation in the Monterey Bay area, *Cont. Shelf Res.*, *22*, 1129–1151.

Skogsberg, T. (1936), Hydrography of Monterey Bay, California: Thermal conditions, 1929–1933. *Trans. Am. Philos. Soc.*, *29*, 152 pp.

Skogsberg, T., and A. Phelps (1946), Hydrography of Monterey Bay, California. Thermal conditions, part II, 1934–1937, *Proc. Am. Philos. Soc.*, *90*, 350–386.

Smith, R. D., J. K. Dukowicz, and R. C. Malone (1992), Parallel ocean general circulation modeling, *Physica D*, *60*, 38–61.

Song, Y. H., and D. Haidvogel (1994), A semi-implicit ocean circulation model using a generalized topography-following coordinate system, *J. Comput. Phys.*, *115*, 228–244.

Tisch, T. D., S. R. Ramp, and C. A. Collins (1992), Observations of the geostrophic current and water mass characteristics off Point Sur, California, from May 1988 through November 1989, *J. Geophys. Res.*, *97*, 12,535–12,555.

Traganza, E. D., V. M. Silva, D. M. Austin, W. L. Hanson, and S. H. Bronsink (1983), Nutrient mapping and recurrence of coastal upwelling centers by satellite remote sensing: Its implication to primary production and the sediment record, in *Coastal Upwelling*, edited by E. Suess and J. Thiede, pp. 61–83, Springer, New York.

Tseng, Y. H. (2003), On the development of a ghost-cell immersed boundary method and its application to large eddy simulation and geophysical fluid dynamics, Ph.D. thesis, Stanford Univ., Stanford, Calif.

Tseng, Y. H., and D. E. Dietrich (2006), Entrainment and transport in the three-dimensional idealized gravity current simulation, *J. Atmos. Oceanic Technol.*, *23*, 1249–1269.

Tseng, Y. H., and J. H. Ferziger (2001), Effects of coastal geometry and the formation of cyclonic/anticyclonic eddies on turbulent mixing in upwelling simulation, *J. Turbul.*, *2*, 014.

Tseng, Y. H., and J. H. Ferziger (2003), A ghost-cell immersed boundary method for flow in complex geometry, *J. Comput. Phys.*, *192*, 593–623.

Tseng, Y. H., and J. H. Ferziger (2004), Large-eddy simulation of turbulent wavy boundary flow: Illustration of vortex dynamics, *J. Turbul.*, *5*, 034.

Tseng, Y. H., D. E. Dietrich, and J. H. Ferziger (2005), Regional circulation of the Monterey Bay region: hydrostatic versus nonhydrostatic modeling, *J. Geophys. Res.*, *110*, C09015, doi:10.1029/2003JC002153.

Wong, F. L., and S. E. Eittreim (2001), Continental shelf GIS for the Monterey Bay National Marine Sanctuary, *U.S. Geol. Surv. Open File Rep.*, *01-179*.

L. C. Breaker, Moss Landing Marine Laboratory, 8272 Moss Landing Road, Moss Landing, CA 95039, USA.

Y.-H. Tseng, Department of Atmospheric Sciences, National Taiwan University, No. 1, Sec. 4 Roosevelt Road, Taipei, 106, Taiwan. (yhtseng@as.ntu.edu.tw)